Computational Fluid Dynamics Analysis of Air Flow and Temperature Distribution in Buildings

Undergraduate Honors Thesis

Presented in Partial Fulfillment of the Requirements for

Graduation with Distinction in Mechanical Engineering

By

Bradley S. Hurak

Defense Committee:

Professor Sandip Mazumder

Professor Yann Guezennec

Abstract

Energy consumption for the heating and cooling of residential buildings accounts for nearly half of total use. Because the physical configuration of heating and cooling inlets and outlets is often determined from historical practice or convenience rather than optimal performance, it stands to reason that there is an opportunity to gain effectiveness of these systems by applying engineering principles to their design. In this study, a computational fluid dynamic analysis was performed to investigate the effect of the physical configuration of inlet and outlet vents on the temperature and flow patterns inside a room modeled for simplicity as a two dimensional enclosure. It was determined that for use in both heating and cooling of a room, a low or floor located inlet vent coupled with an outlet that is positioned on the upper half of a wall yields the most desirable results in reaching, or nearly reaching, comfort conditions in the shortest amount of time. However, if either heating or cooling is expected to be the primary energy consumption, it may be advantageous to deviate from this configuration.

Acknowledgements

I would like to thank everyone who has supported me throughout the course of this project. I am appreciative for the help and patience of my advisor, Professor Sandip Mazumder. I have valued and learned from the constructive criticism that Professor Yann Guezennec has offered throughout the classroom sessions for this project. ESI Group is also acknowledged for providing lisences to their commercial software, CFD-ACE+. Finally, I am very grateful for the encouragement, support, and love that my parents have always given me.

Table of Contents

List of Figures

List of Tables

1 Introduction

Although energy consumption per household decreased 31% from the year 1978 until 2005 in the United Stated, the rise in the total number of homes results in an only slight decrease in total residential energy use per year, from 10.58 quadrillion BTU to 10.55 quadrillion BTU, respectively. Heating and cooling costs account for a significant portion of this consumption; specifically, heating is identified as accounting for 41% of total residential energy consumption while air conditioning accounts for 8%. The consequence of this energy consumption pattern is that nearly half of the energy consumed in the residential sector is used by heating and cooling. It follows that with such a substantial portion of energy consumption in this area, any gain in efficiency or design of heating and cooling systems would result in a decrease in energy usage leading to reduced costs and, since most of the energy produced in the United States causes the production of greenhouse gases, reduced greenhouse emissions.

Heating, ventilating and air conditioning (HVAC) systems are often designed by architects from experience, historical practice, and convenience. In order to reduce heating and cooling energy consumption by increasing the effectiveness of these systems, it would be advantageous to have a set of standardized design principles to guide the design of HVAC systems.

1.1 Literature Survey

While many CFD studies have been conducted to determine flow patterns in buildings or to determine ideal control methods for HVAC systems, there were no studies found that investigated the effect of changing the vent locations in a living area. Also, no standards of vent configuration design were found. However, the following studies were useful in setting up proper CFD models for the purposes of this research.

A study by K. C. Chung was used extensively in the initial stages of this research because of the amount of data that was provided; Chung's three-dimensional investigation into airflow in a partitioned environment provided a basis for a preliminary examination of potential models to be studied. Chung's study included a detailed three-dimensional model that showed with velocities at various planes and temperature contours in those same planes. Additionally, details of the CFD model inputs were provided. However, in attempts to validate a model that was planned to be used in this current study, some vague model inputs and convergence problems did not allow a replication of the results. Accordingly, this preliminary CFD model validation attempt was dismissed.

The study by Sun et al. also provides a model of a CFD study of an indoor environment. A dynamic simulation was used to evaluate HVAC control systems based on a CFD model of a room, a mathematically modeled PID controller, and an actuation model. While the control model was beyond the scope of this current research, the CFD model was a helpful guide in gauging model inputs.

1.2 Objectives of Current Research

The goal of this study is to evaluate different ventilation configurations in a single room. By analyzing the results of the simulations, it was intended to develop a criterion that would help to improve ventilation efficiency simply by ensuring that the physical configuration of the inlet and outlet vents was maximized under both heating and cooling conditions. In this way, the effectiveness of the overall system can be increased without requiring more efficient or more expensive components.

2 Methods

A simple two-dimensional model of a room was analyzed using CFD-ACE+^{TM}, a commercial computational fluid dynamics software package, to examine airflow and temperature distribution under different circumstances. The model was set in summer conditions in which cooling was necessary and in winter conditions in which heating was necessary. In both cases, the position of the inlet and outlet vents was parametrically changed yielding a large matrix of results.

Additionally, a three-dimensional model was developed in much the same way as the two-dimensional model. With the same number of inlet and outlet locations as the two-dimensional case, a parametric study was planned; however, computing time and convergence problems prevented this study from being completed.

2.1 Two-dimensional Model Description

A two-dimensional model of a rectangular room with a width of 12 feet and a height of 10 feet was used to create a mesh with a density of approximately 7.5 nodes per linear foot. The resulting mesh was 74 nodes wide by 92nodes high with a total of 6808 nodes. Additionally, the boundaries of the mesh were split into parts yielding ten one-foot-long sections that were used as inputs and outputs. Of these sections, the inputs were located as follows: one inlet was located on the ceiling at 0.5 feet from the left wall, one inlet was located on the floor at 0.5 feet from the left wall, and three inlets were located on the left wall at 0.5 feet from the floor and ceiling and midway up the wall centered at 5 feet. The outlets were similarly located on the right side of the two-dimensional model. Also, a temperature monitor point that was used to determine the transient temperature at a location that would correspond to a person sitting in a chair in the middle of the room was set at 3 feet above the floor and 6 feet from either side wall. Figure 1 shows the geometry of the two-dimensional model, including the locations of the inlets, which are denoted by the notation “I#”, where “I” stands for “inlet” and “#” is the number

given to the inlet location, the outlets, which are similarly marked with the notation “O#”, and the placement of the temperature probe, which is indicated with a “+”.

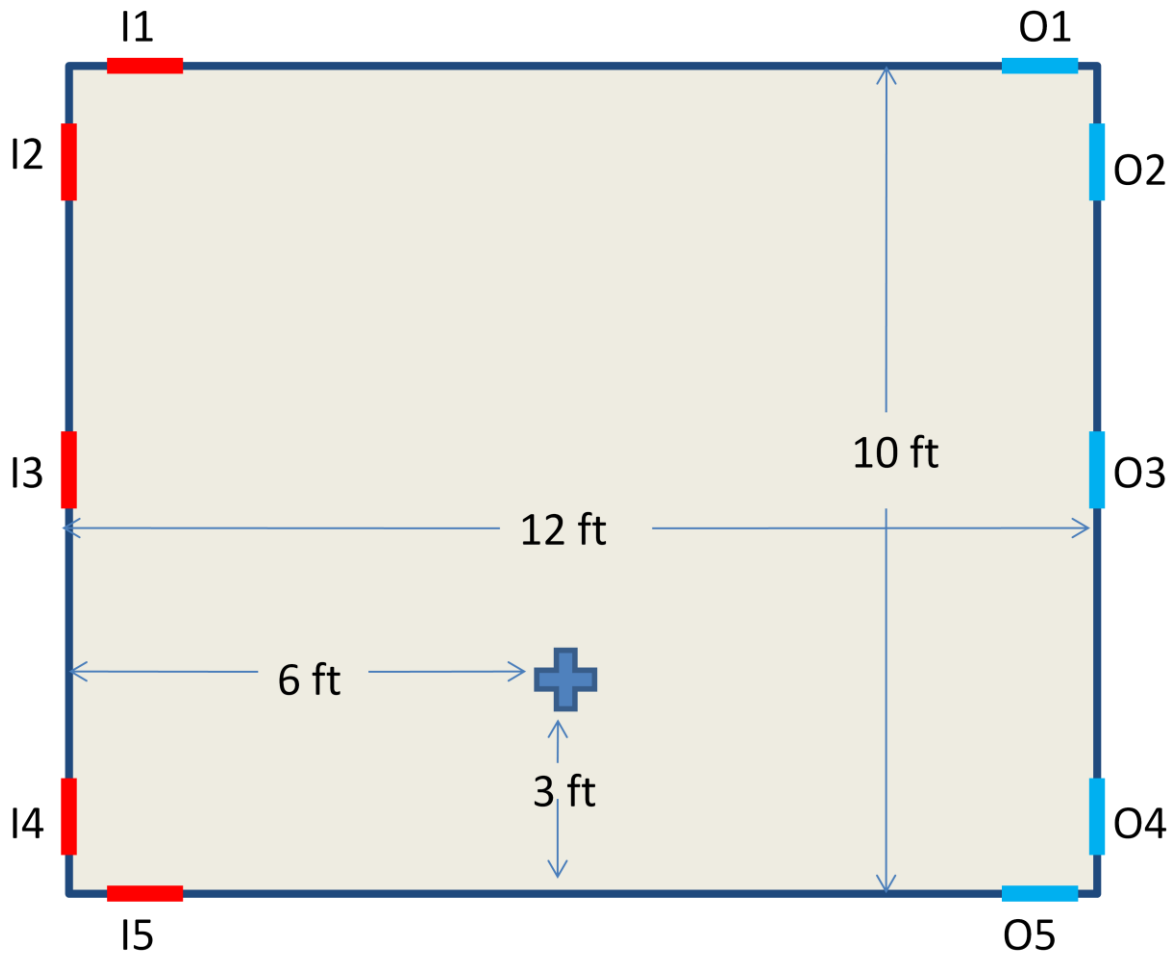

Figure 1: Two-dimensional model with inlets, outlets, and temperature probe.

2.2 Three-dimensional Model Description

A three-dimensional model of a room in the shape of a rectangular prism was developed. The physical dimensions were set to be 12 feet wide by 12 feet long by 10 feet tall. The resulting mesh had approximately 5 nodes per linear foot, yielding a three-dimensional mesh of 152,460 nodes, or 82,080 cells. This model also had inlet and outlet configurations that were analogous to the two-dimensional case. The inlets were located in one corner of the room while the outlets were in the opposite corner. The highest vent, for both inlets and outlets, was located in the corner of the ceiling of the model room

at 6 inches from either sidewall. Moving down the wall, a vent was located at 6 inches below the ceiling and 6 inches from the sidewall while another vent was 6 inches above the floor and 6 inches from the sidewall. Also, there was a vent that was positioned in the middle of the height of the wall, centered at 5 feet from the floor and with one edge 6 inches from the sidewall. Finally, another vent was located on the floor at 6 inches from either sidewall. The inlets were sized at 1 foot by 1 foot while the outlets were 2 feet by 1 foot. A diagram of the three-dimensional model is shown in Figure 2. The inlets and outlets are similarly identified as in the two-dimensional case presented above.

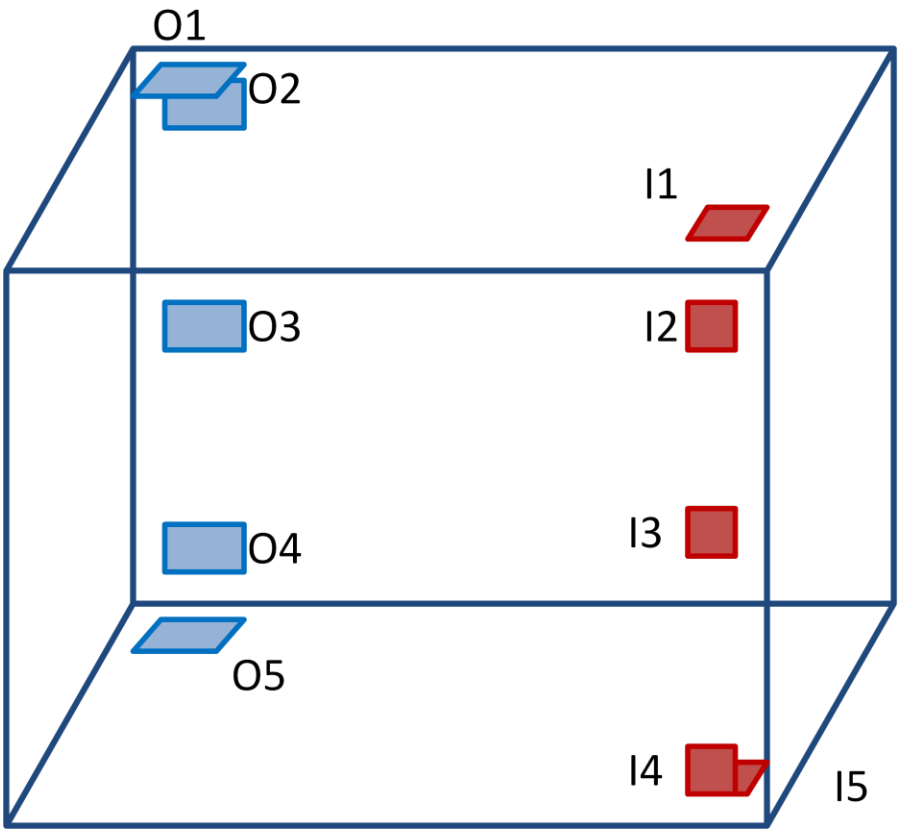

Figure 2: Three-dimensional model with inlets and outlets.

2.3 Parametric Study

Using CFD-ACE+, twenty five geometrically different cases were studied to evaluate the fluid flow and temperature distributions within the two-dimensional model room. These cases were

parametrically determined from the above model; using only one inlet and one outlet for each simulation, the inlets and outlets were changed one at a time so that each case evaluated the model for a distinct combination of inlets and outlets.

Table 1 below identifies the twenty five test configurations that were considered.

Table 1: List of test numbers according to inlet and outlet position.

Inlet → / Outlet ↓	1	2	3	4	5
1	1-1	2-1	3-1	4-1	5-1
2	1-2	2-2	3-2	4-2	5-2
3	1-3	2-3	3-3	4-3	5-3
4	1-4	2-4	3-4	4-4	5-4
5	1-5	2-5	3-5	4-5	5-5

2.4 Model Conditions

Each of the cases presented in Table 1 was simulated under hot and cold ambient temperature conditions. In both cases, the target comfort condition was taken to be 295.2 K, or 72 °F, based on industry standards. For the two-dimensional case, transient simulations were carried out at step intervals of 5 seconds for 360 time steps which is equivalent to 30 minutes. For the three-dimensional model, steady state solutions were planned to be studied with transient analyses to follow. A description of the conditions and assumptions is given in the following sections.

2.4.1 Hot Conditions

The hot conditions were meant to simulate a hot summer day. As such, a temperature of 308 K, or about 95 °F, was chosen as the outside air temperature. Additionally, the ground temperature was assumed to be cooler at 290 K, or approximately 62 °F. The initial temperature inside the room was taken to be equal to the external ambient condition at 308 K. The inlet temperature of the model vents was set to be 2.3 K above the comfort condition at 298.5 K, or 77.6 °F.

2.4.2 Cold Conditions

The cold conditions were chosen to replicate cold winter temperatures. Thus, the ambient temperature was set to 266.5 K, or 20 °F. Also, the ground temperature was set slightly lower than the summer ground condition at 286, or 55 °F. Because heating is not completely turned off in cold conditions, the initial air temperature inside the room was taken to be 286 K. The inlet temperature was set to be 2.2 K below the comfort condition at 292 K, or about 66 °F.

3 CFD Model

The CFD package, CFD-ACE+, was set up to use three modules to resolve the flow and temperature distributions of the model: flow, heat transfer, and turbulence. Each of these three modules has its own set of governing equations and is discussed in its respective section below. While the equations presented apply directly to the two-dimensional cases, the three-dimensional cases require an equivalent set of three-dimensional equations.

3.1 Flow Module

The flow module determines the velocity and pressure fields by solving the two-dimensional momentum equations and the pressure correction equations, respectively. These equations are guided by the laws of conservation of mass and momentum, which lead to the use of the Navier-Stokes equations to iteratively resolve the flow solutions. The following sections describe the governing flow equations.

3.1.1 Mass Conservation Equation

The law of conservation of mass is applied to the model room which serves as the control volume; accordingly, the time rate of change of mass in the room must be balanced by the difference between the mass exiting and entering the room. This principle is described by the equation below.

$$\frac{\partial \rho}{\partial t} + \nabla \bullet \left(\rho \vec{V}\right) = 0 \qquad (1)$$

where ρ is the air density and $\vec{V}$ is the velocity vector. The first term on the left expresses the time rate of change of density while the second term describes the net mass flow through the control volume.

3.1.2 Momentum Conservation Equations

The law of conservation of momentum must also be applied; this states that the time rate of change of momentum of a fluid element is equal to the sum of the forces acting on the element. The equation below describes the two-dimensional x-component of this principle.

$$\frac{\partial(\rho u)}{\partial t} + \nabla \bullet \left(\rho \vec{V} u\right) = \frac{\partial(-p + \tau_{xx})}{\partial x} + \frac{\partial \tau_{xy}}{\partial y} + S_{Mx} \tag{2}$$

where u is the fluid velocity in the x-direction, p is the pressure, τ is the viscous stress, and S is the rate of increase in momentum caused by forces on the element. The left side of the equation is the rate of change of momentum in the x -direction while the left side describes the rate of change of total forces on the element in the x-direction. Similarly, the y-component is expressed below.

$$\frac{\partial(\rho v)}{\partial t} + \nabla \bullet \left(\rho \vec{V} v\right) = \frac{\partial \tau_{xy}}{\partial x} + \frac{\partial\left(-p + \tau_{yy}\right)}{\partial y} + + S_{My} \tag{3}$$

where v is the fluid velocity in the y-direction.

3.1.3 Navier-Stokes Equations

To further develop the momentum equations given above, the variable viscous stresses for two-dimensional flows are defined below.

$$\tau_{xx} = 2\mu \frac{\partial u}{\partial x} - \frac{2}{3}\mu\left(\nabla \bullet \vec{V}\right) \tag{4}$$

$$\tau_{yy} = 2\mu \frac{\partial v}{\partial y} - \frac{2}{3}\mu\left(\nabla \bullet \vec{V}\right) \tag{5}$$

$$\tau_{xy} = \tau_{yx} = \mu\left(\frac{\partial u}{\partial y} + \frac{\partial v}{\partial x}\right) \tag{6}$$

Combining equations 9 through 11 with momentum equations 7 and 8 results in the Navier-Stokes equations which are presented below.

$$\frac{\partial(\rho u)}{\partial t} + \nabla \bullet \left(\rho \vec{V} u\right) = -\frac{\partial p}{\partial x} + \frac{\partial}{\partial x}\left[2\mu \frac{\partial u}{\partial x} - \frac{2}{3}\mu\left(\nabla \bullet \vec{V}\right)\right] + \frac{\partial}{\partial y}\left[\mu\left(\frac{\partial u}{\partial y} + \frac{\partial v}{\partial x}\right)\right] + S_{Mx} \tag{7}$$

$$\frac{\partial(\rho v)}{\partial t} + \nabla \bullet \left(\rho \vec{V} v\right) = -\frac{\partial p}{\partial y} + \frac{\partial}{\partial x}\left[\mu\left(\frac{\partial u}{\partial y} + \frac{\partial v}{\partial x}\right)\right] + \frac{\partial}{\partial y}\left[2\mu\frac{\partial v}{\partial y} - \frac{2}{3}\mu(\nabla \bullet \vec{V})\right] + S_{My} \quad (8)$$

These above equations can be simplified and rewritten as the following equations.

$$\frac{\partial(\rho u)}{\partial t} + \nabla \bullet \left(\rho \vec{V} u\right) = -\frac{\partial p}{\partial x} + \nabla \bullet (\mu \nabla \mathrm{u}) + S_{Mx} \quad (9)$$

$$\frac{\partial(\rho v)}{\partial t} + \nabla \bullet \left(\rho \vec{V} v\right) = -\frac{\partial p}{\partial y} + \nabla \bullet (\mu \nabla \mathrm{v}) + S_{My} \quad (10)$$

3.1.4 Other Flow Properties

The following table shows the fluid properties that were held constant and used to calculate other model parameters.

Table 2: Flow Model Constants.

Parameter	Symbol	Value
Reference Pressure	p_{ref}	101325 Pa
Universal Gas Constant	R	8.314472 J/mol K
Molecular Weight of Air	MW	29 kg/kmol
Dynamic Viscosity	μ	$1.846(10^{-5})$ kg/m s
Specific Heat	C_p	1007 J/kg K
Thermal Conductivity of Air	k_{air}	0.0263 W/m K

Using the above values, other variable model parameters were calculated within the CFD simulation. These calculations include the fluid density and the kinematic viscosity. The fluid density was calculated using the Ideal Gas Law. This equation is given below.

$$\rho = \frac{(p + p_{ref})MW}{R \cdot T} \quad (11)$$

where ρ is density, p is pressure and T is the temperature of the air. Also, the kinematic viscosity was calculated with the following equation.

$$\nu = \frac{\mu}{\rho} \tag{12}$$

3.2 Heat Transfer Module

The heat transfer module was used to calculate the temperature distribution within the model room as well as the interactions with the environment. These calculations were performed according to the law of conservation of energy. The equation that was solved in CFD-ACE+ was the total enthalpy equation, which is given below.

$$\frac{\partial(\rho h_o)}{\partial t} + \nabla \bullet \left(\rho \vec{V} h_o\right) = \nabla \bullet \left(k_{eff} \nabla \mathrm{T}\right) + \frac{\partial p}{\partial t} + \left[\frac{\partial(u\tau_{xx})}{\partial x} + \frac{\partial\left(u\tau_{yx}\right)}{\partial y}\right] + \left[\frac{\partial\left(v\tau_{xy}\right)}{\partial x} + \frac{\partial\left(v\tau_{yy}\right)}{\partial y}\right] \tag{13}$$

where h_o is the total enthalpy which is defined as:

$$h_o = i + \frac{p}{\rho} + \frac{1}{2}(u^2 + v^2) \tag{14}$$

where i is the internal energy, k_{eff} is the effective thermal conductivity, p is the static pressure, and τ is the viscous stress tensor which was described in equations 9 through 11, above.

3.2.1 Thermal Boundaries

In addition to the above equations, it was necessary to define the conditions at the walls of the room to determine the thermal interaction with the ambient temperature outside of the model. The boundary consisted of three different elements: the ceiling, the walls, and the floor. While each of these sections had distinct thermal properties, a similar method of determining the effective heat transfer coefficients of each part was used. In general, an overall heat transfer coefficients was calculated using a thermal resistance model which took into account the conductive heat transfer within each layer of the boundary walls and the convective heat transfer to the ambient environment, if applicable. Overall, the heat transfer rate through the room's boundaries can be expressed as follows:

$$q = h_{eff} \cdot A \cdot \left(T_w - T_{inf}\right) \quad (15)$$

where q is the heat transfer rate, h_{eff} is the overall heat transfer coefficient, A is the area of the boundary, T_w is the temperature on the inside of the boundary, and T_{inf} is the ambient temperature. Subsequently, the over heat transfer coefficient, h_{eff}, is defined as the reciprocal of the sum of the thermal resistances at the boundary, as shown in the equation below.

$$h_{eff} = \frac{1}{R_{total}} \quad (16)$$

where the R_{total} is the combined conductive and convective thermal resistances, R_c and R_h, respectively. These properties are defined in the following equations.

$$R_c = \frac{L}{k} \quad (17)$$

where k is the material specific thermal conductivity and L is the thickness of the material layer.

$$R_h = \frac{1}{h_{inf}} \quad (18)$$

where h_{inf} is the convective heat transfer coefficient of air.

Detailed below are the assumptions, values, and calculations used for each of these three sections.

3.2.1.1 Ceiling Thermal Properties

The ceiling was simply modeled as three different layers of material and an external convective heat transfer layer as is shown in Figure 3, below. The type, thermal properties, and thickness of each of the materials is shown in the table below.

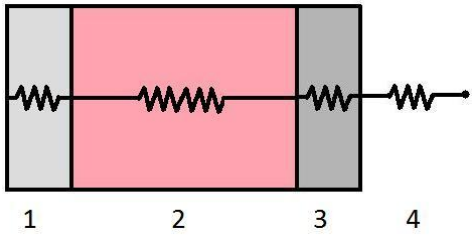

Figure 3: Thermal resistance model of ceiling.

Table 3: Material type, thermal properties and thickness of ceiling thermal model layers.

Layer	Material	Thermal Properties	Thickness
1	Drywall	k=0.1700 W/mK	15.875 mm
2	Air	k=0.0263 W/mK	304.8 mm
3	Plywood	k=0.1200 W/mK	15.875 mm
4	Air (ambient)	h_{inf}=10 W/m^{2}K	NA

Using this thermal resistance model and equations 3 and 4, the total thermal resistance of the ceiling was calculated as follows:

$$R_{total} = \sum R_c + \sum R_h = \frac{L_1}{k_1} + \frac{L_2}{k_2} + \frac{L_3}{k_3} + \frac{1}{h_{inf}} \quad (19)$$

Inserting the respective values yields a total thermal resistance of 11.915 m^{2}K/W. The reciprocal of this thermal resistance, as has been shown in equation 2, is the overall heat transfer coefficient of the ceiling, $h_{ceiling}$, or 0.0839 W/m^{2}K.

3.2.1.2 Wall Thermal Properties

The thermal model of the walls consisted of four layers of material and an outer convective heat transfer layer. This concept is shown in Figure 4 and the layer properties are shown in Table 4 below.

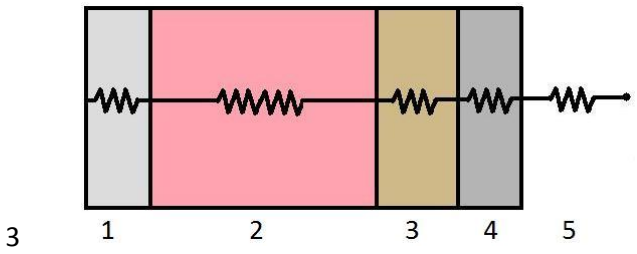

Figure 4: Thermal resistance model of side walls.

Table 4: Material type, thermal properties and thickness of side wall thermal model layers.

Layer	Material	Thermal Properties	Thickness
1	Drywall	k=0.1700 W/mK	15.875 mm
2	Air	k=0.0263 W/mK	101.60 mm
3	Plywood	k=0.1200 W/mK	15.875 mm
4	Siding	k=0.0940 W/mK	15.875 mm
5	Air (ambient)	h=10 W/m^2K	NA

Using the above information and equations 2 through 4 as applied in the previous section, the overall heat transfer coefficient of the side walls, h_{wall}, was determined to be 0.3699 W/m^2K.

3.2.1.3 Floor Thermal Properties

Again, a similar thermal resistance model is used for the floor with the exception of the convective heat transfer term which is not included in the formulation. Figure 5 shows that the floor was taken to have five layers of material to a depth of approximately 6.5 feet, a depth at which the ground temperature is considered to be constant. Table 5 shows the thermal and dimensional properties of the material layers.

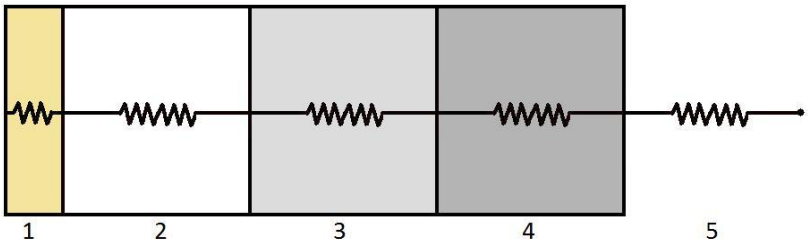

Figure 5: Thermal resistance model of floor.

Table 5: Material type, thermal properties and thickness of floor thermal model layers.

Layer	Material	Thermal Properties	Thickness
1	Wood	k=0.120 W/mK	25.4 mm
2	Air	k=0.0263 W/mK	152.4 mm
3	Sand/Gravel	k=1.0 W/mK	152.4 mm
4	Concrete	k=1.4 W/mK	152.4 mm
5	Clay	k=1.3 W/mK	1.524 m

Using the information above, along with Equations 2 through 4, the overall heat transfer coefficient for the floor of the room, h_{floor}, was determined to be 0.1332 W/m^{2}K.

3.3 Turbulence Module

The CFD program was set to use a standard k-epsilon model for turbulence. The required input variables were the turbulent kinetic energy, K, and the turbulent dissipation, d. The equations used to find these values are presented

$$K = \frac{3}{2}(U \cdot I)^2 \tag{20}$$

where U is the flow velocity at the inlet and I is the turbulence intensity. The inlet flow velocity was taken to be 1.5 air changes per hour, or ACH, meaning that the total volume of the room would be replaced 1.5 times in one hour. The formulation for the inlet flow velocity, U, is shown below.

$$U = \frac{\dot{V}}{w} \tag{21}$$

where $\dot{V}$ is the required volumetric flow rate as calculated from equation 4 below and w is the width of the inlet.

$$\dot{V} = 1.5ACH = 1.5\frac{W \cdot H}{1\ hour} \tag{22}$$

where W is the room width and H is the room height. Inserting the respective values yields a volumetric flow rate, $\dot{V}$, equal to 16.7225 m^2/hr, or 0.0046 m^2/s. Plugging this value into equation 3 yields an inlet

velocity, U, of 0.01524 m/s. This inlet flow velocity can be directly inserted into equation 6, with a turbulence intensity value of 0.05, to result in a turbulent kinetic energy value, K, of 8.71(10^{-7}) m^2/s^2.

Next, the turbulent dissipation, d, can be calculated using the equation 5.

$$d = C_{\mu}^{\frac{3}{4}}\left(\frac{K^{\frac{3}{2}}}{l}\right) \tag{23}$$

where C_μ is a turbulence model constant of 0.09 and l is the turbulent length scale which is defined below.

$$l = 0.03L \tag{24}$$

where L is the characteristic length of the inlet. Using these relationships and the values above, the turbulent dissipation was calculated to be 1.4606(10^{-8}) m^2/s^3.

3.4 Three-dimensional Model Properties

Using the same formulations as presented above, the three-dimensional model properties that were different from the two-dimensional case are given in Table 6.

Table 6: Three-dimensional model parameters.

Parameter	Symbol	Value
Inlet Velocity	U	0.18288 m/s
Turbulent Kinetic Energy	K	0.0084375 m^2/s^2
Turbulent Dissipation	d	0.0033215737 m^2/s^3

4 Results

The twenty five two-dimensional test cases were run under both hot and cold conditions. The data collected included the temperature data at the monitor point and the temperature distribution at all node points in the model room at the end of the 30 minute simulation. The normalized residuals of all computations were required to be at a 0.001 level. Under some cases, however, this level of convergence was not attained. If the residuals were below the acceptable level for a significant length of time, these simulations may be considered up to the point at which the solution began to diverge. Otherwise, if the solution only converged for a small number of time steps, these cases were excluded from the following discussion.

For the three-dimensional model, steady state simulations were carried out, but convergence was difficult to achieve as the normalized residuals were required to fall below four orders of magnitude. For that reason, the results that were obtained were not considered to be valid and are not included in this analysis.

4.1 Flow Data

Some general observations can be made about the flow patterns that apply to both the hot and cold conditions. Most notably, natural convection often had the strongest influence on the temperature and flow patterns of the simulations. It was observed that under conditions in which a cooling vent was placed near the top of a room and the outlet was also near the top, the cool incoming air would be directed along the nearest side wall to the floor where it would slowly fill the room. This case is analogous to the filling of a bucket with water. This flow pattern, which was dominated by natural convection, showed a lack of penetration of the heating or cooling air which in turn inhibited the incoming air from mixing with the room air. As a result, this general vent configuration was shown to give favorable results for cooling while showing poor results for cooling. The opposite was true if a

heating inlet was placed near the bottom of the room; the flow would quickly divert to the nearest wall where it would rise to the ceiling. If the outlet was also placed near the bottom of the room, the room would become filled with this warmer air from top to bottom. An example of the natural convection flow and temperature pattern under cooling effect is shown in Figure 6. The incoming cool and relatively dense air almost immediately sinks to the floor where it only rises to the level of the outlet vent. Only the bottom portion of the room is cooled while the top stays close to the initial condition of 308 K. Additionally, while there is some degree of cooling that occurs near the floor, both the monitor point and the volume averaged temperature are above the comfort condition at over 305 K. Thus, since this option offers less than 3 K of cooling, it is clearly not an ideal configuration for cooling.

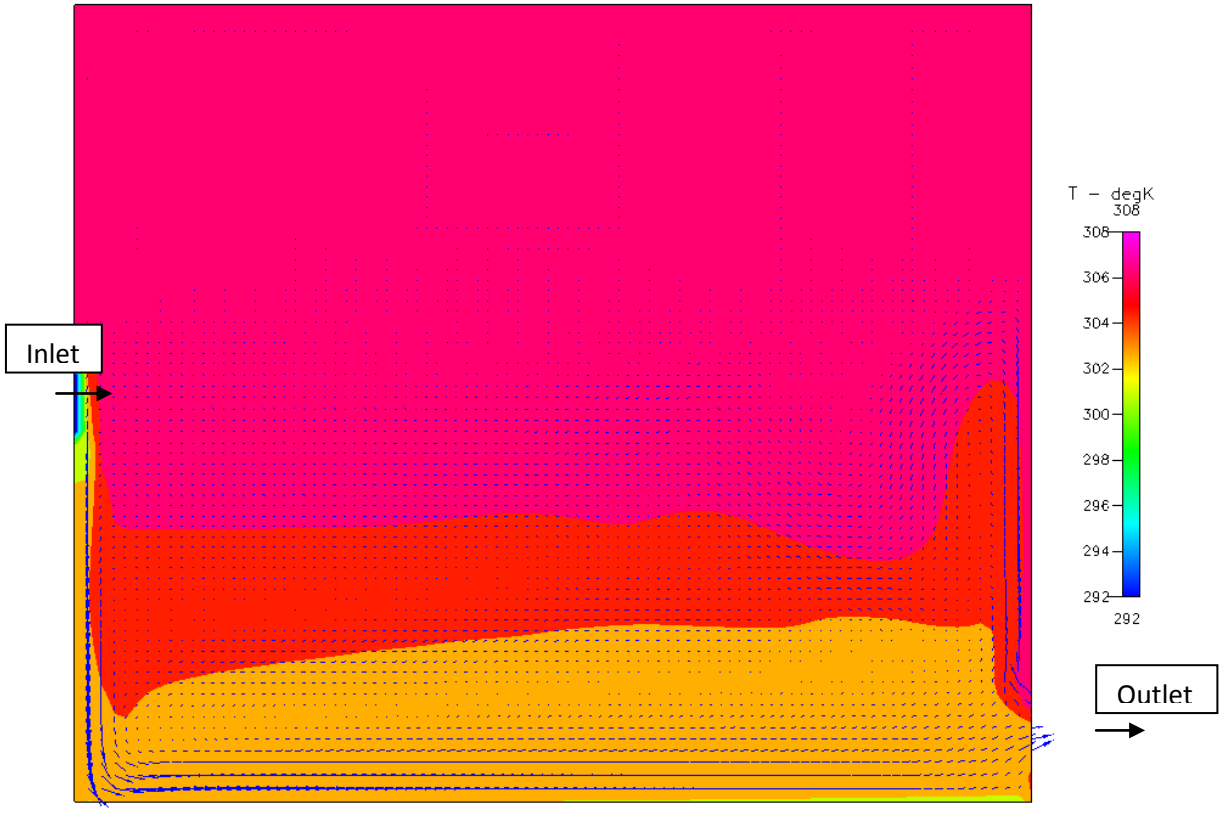

Figure 6: Configuration 3-4, Cooling.

4.2 Temperature Data

Figure 7 through Figure 11 below show the transient temperature data at the monitor point for each configuration with inlet 2. Also, Table 7 shows the final temperature at the monitor point and the volume averaged temperature for each of the configurations with inlet 2.

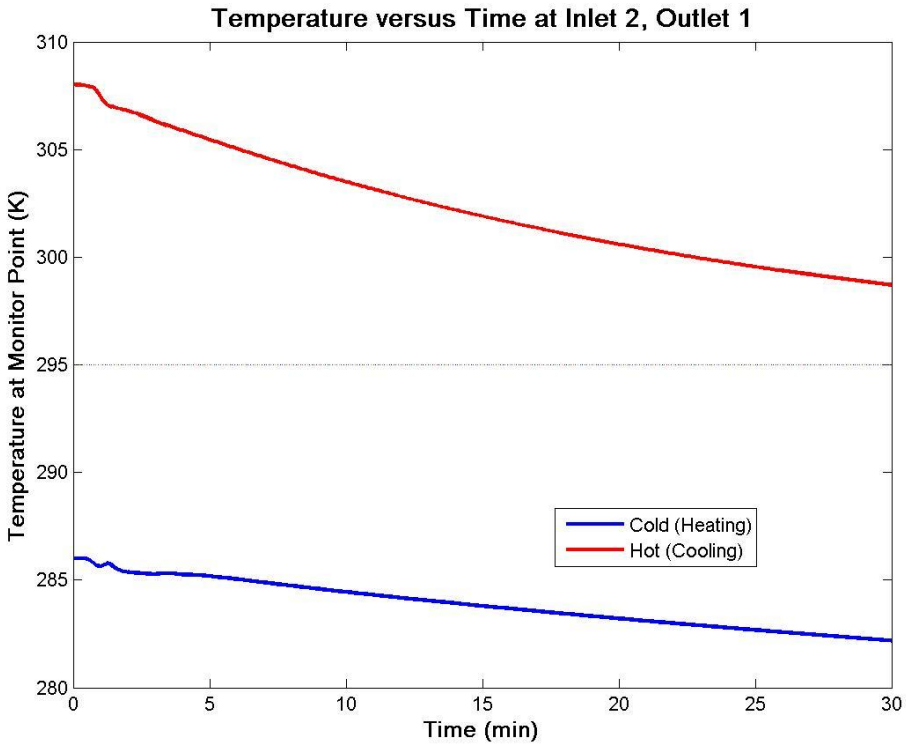

Figure 7: Monitor point temperature data, Inlet 2, Outlet 1.

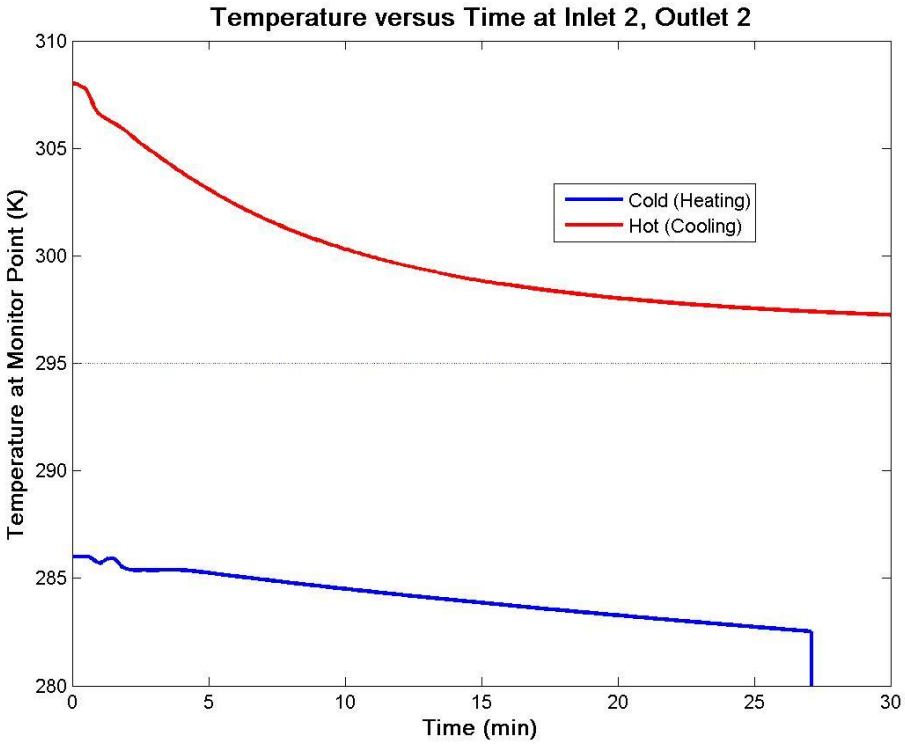

Figure 8: Monitor point temperature data, Inlet 2, Outlet 2.

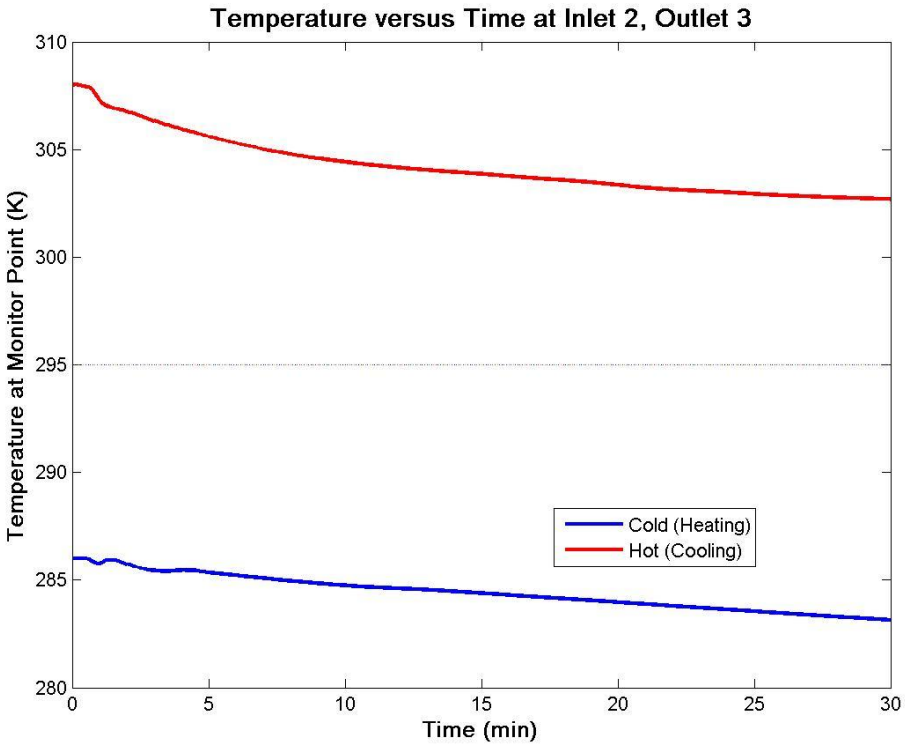

Figure 9: Monitor point temperature data, Inlet 2, Outlet 3.

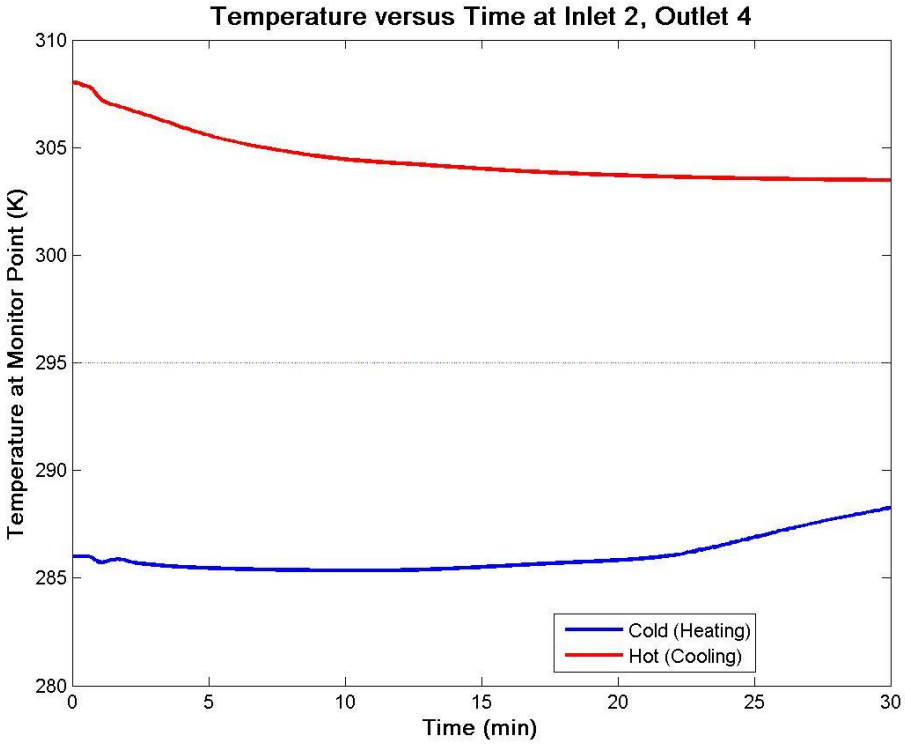

Figure 10: Monitor point temperature data, Inlet 2, Outlet 4.

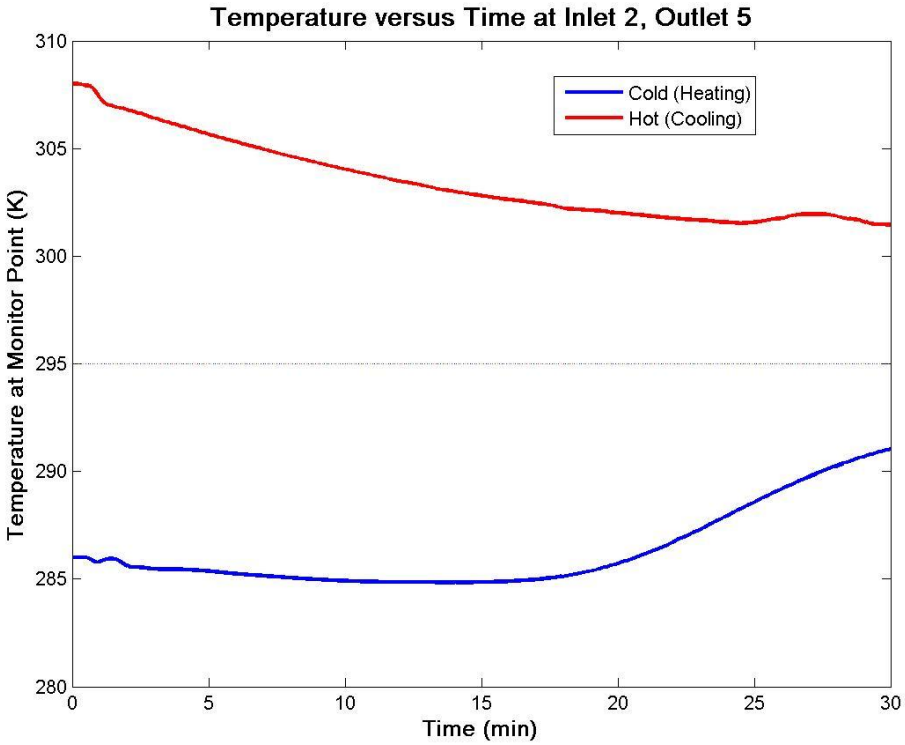

Figure 11: Monitor point temperature data, Inlet 2, Outlet 5.

Table 7: Monitor point and total volume temperature data at end of transient period, Inlet 2.

Test ID	Monitor Point Temperature (K)	Volume Average Temperature (K)
Cold 2-1	282.1926	284.0113
Cold 2-2	282.5266	285.2169
Cold 2-3	283.1474	288.9158
Cold 2-4	288.2422	291.0687
Cold 2-5	291.0074	292.5201
Hot 2-1	298.7191	298.9214
Hot 2-2	297.2531	298.25
Hot 2-3	302.6958	303.4136
Hot 2-4	303.4839	303.7837
Hot 2-5	301.4555	301.6854

By examining this data set, some general trends can be discerned. While none of these configurations reach the desired comfort condition of 295.2 K, the data still provides insights into the patterns of temperature distribution. Looking at the cold condition, it can be seen that as the outlet is lowered from location one to location five, the heating effectiveness is improved. In fact, for outlets one through three, the monitor point temperature declines below the initial temperature of 286 K, while the same is true of the volume average temperature for outlet configurations one and two. Under the hot condition, it can be seen that as the outlet is lowered from outlet position 1 to outlet position 5, the cooling becomes less effective. For both the monitor point, a 6.23 K rise in temperature is seen between the most and least effective configurations while for the overall volume averaged temperature, the rise is 5.53 K. It is important to note that these results show that the desired configurations for cold and hot conditions are the opposite of one another.

Now, by examining the results of all configurations involving outlet 2, other generalizations about the results can be drawn. The following figures show the transient temperature data for at the monitor point for both hot and cold conditions. In addition, Table 8 shows the final monitor point temperature and the volume averaged temperatures for the same simulations.

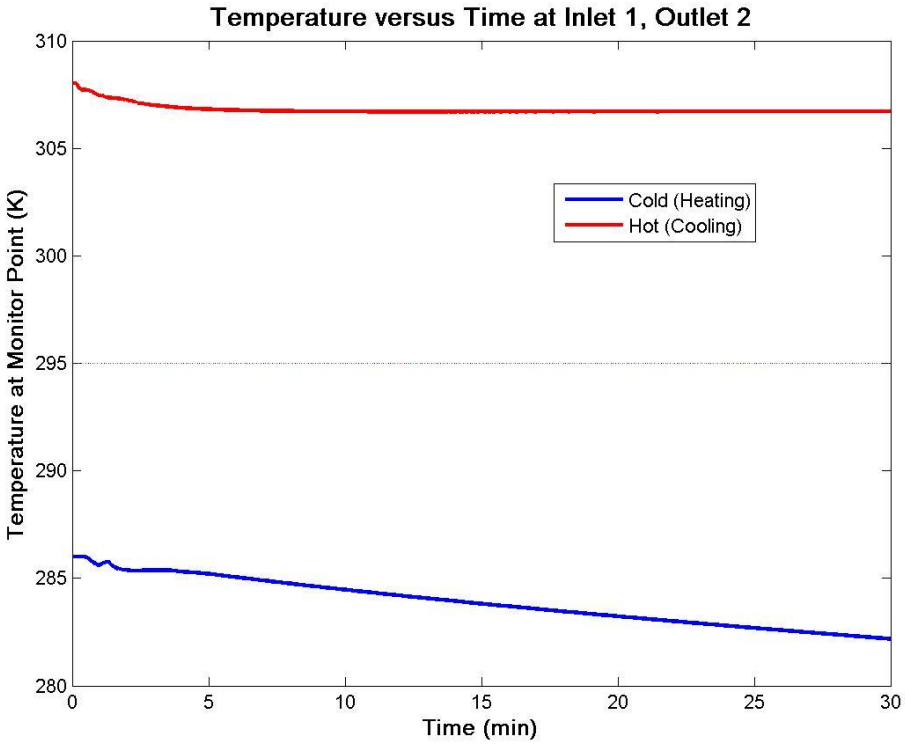

Figure 12: Monitor point temperature data, Inlet 1, Outlet 2.

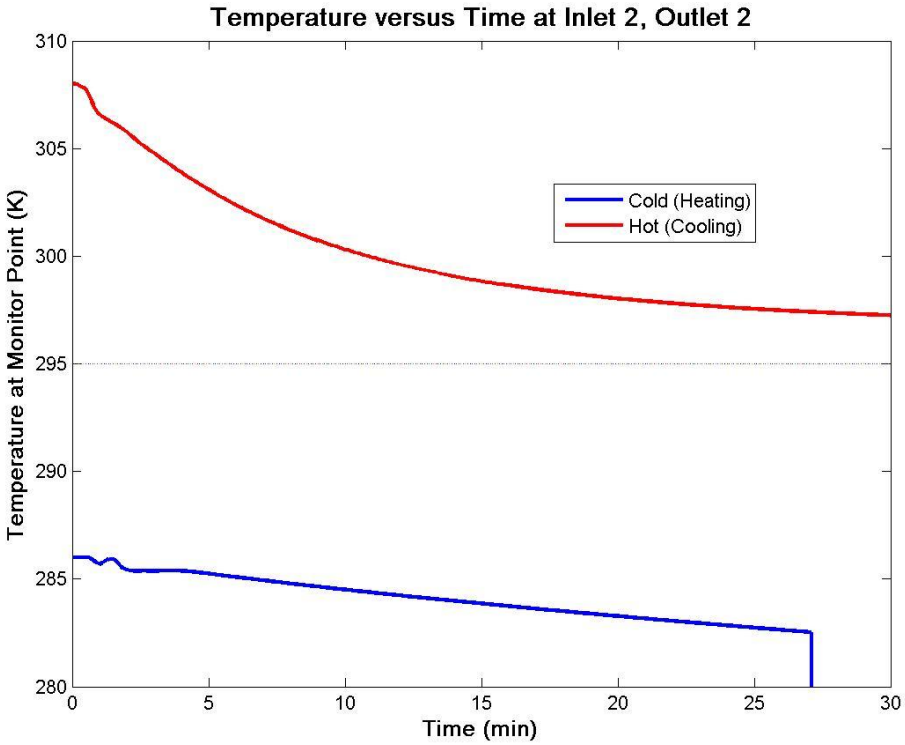

Figure 13: Monitor point temperature data, Inlet 2, Outlet 2.

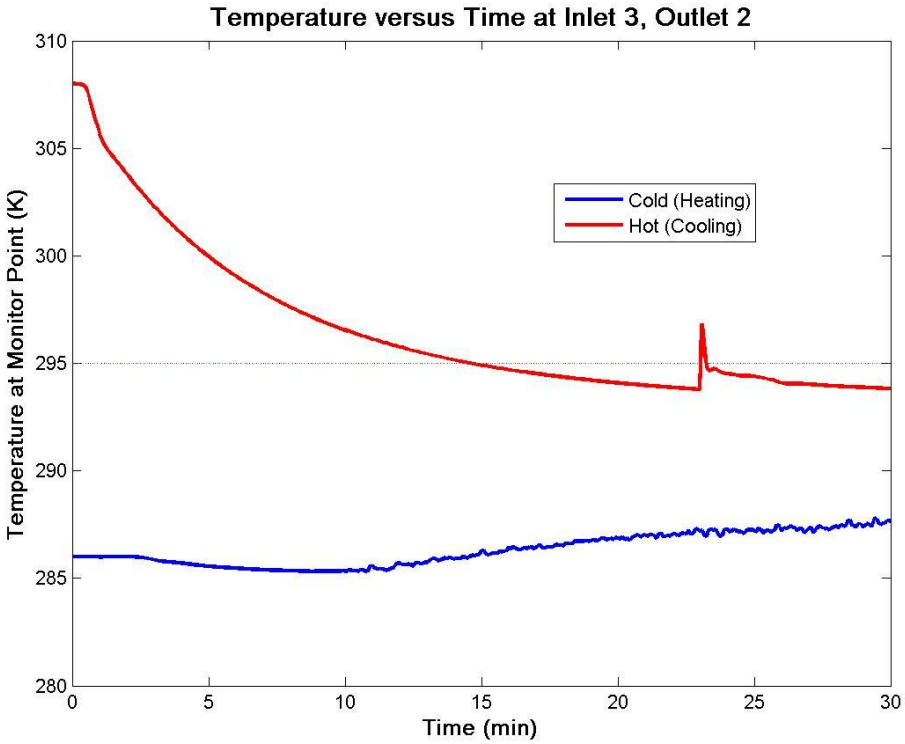

Figure 14: Monitor point temperature data, Inlet 3, Outlet 2.

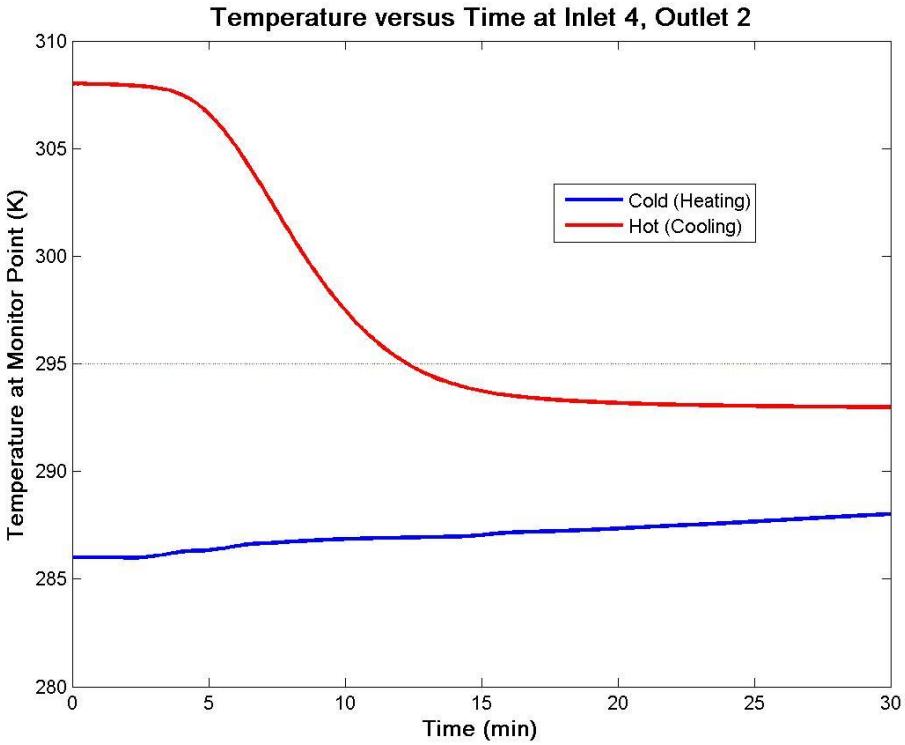

Figure 15: Monitor point temperature data, Inlet 4, Outlet 2.

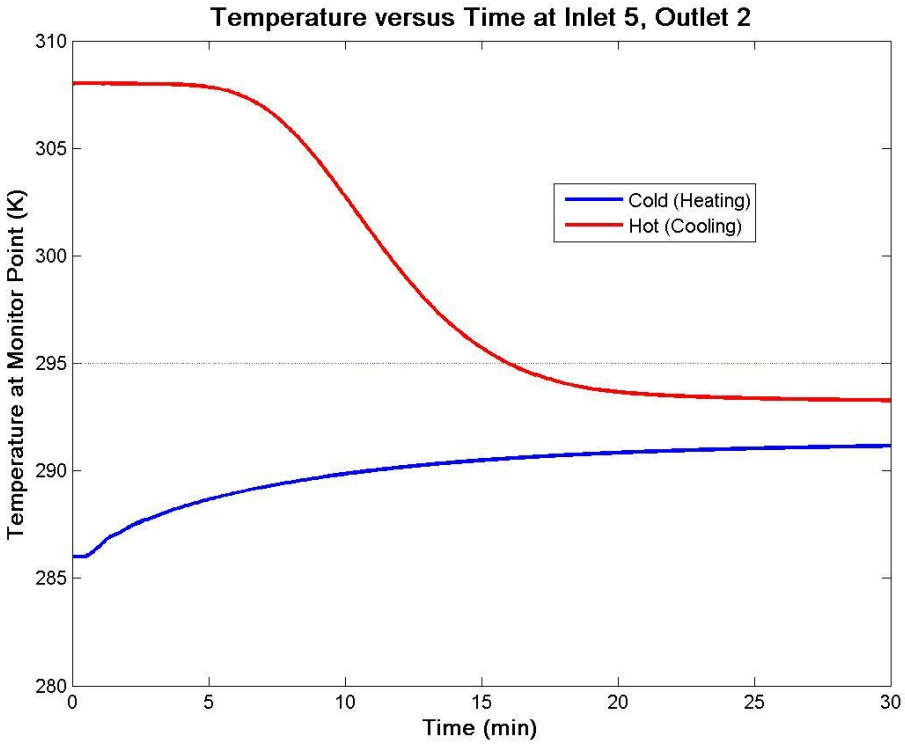

Figure 16: Monitor point temperature data, Inlet 5, Outlet 2.

Table 8: Monitor point and total volume temperature data at end of transient period, Outlet 2.

Test ID	Monitor Point Temperature (K)	Volume Average Temperature (K)
Cold 1-2	282.1886	284.0255
Cold 2-2	282.5266	285.2169
Cold 3-2	287.7024	288.9
Cold 4-2	288.0104	288.2641
Cold 5-2	291.156	291.0623
Hot 1-2	306.697	306.5633
Hot 2-2	297.2531	298.25
Hot 3-2	293.8232	297.1519
Hot 4-2	292.9821	296.2407
Hot 5-2	293.2775	297.0548

This data set makes it possible to draw more generalizations about the results of the simulations. Considering the cold conditions first, it is seen that as the inlet is moved from the top location one to the bottom location five, the heating becomes more effective; at the monitor point, there is a 8.97 K

temperature difference while the volume averaged temperature shows a difference of 7.03 K between the best and worst case scenarios. Furthermore, under the hot conditions, it can be noted that as the inlet location is moved from the top location one to the bottom location five, the cooling becomes more effective. Specifically, the best configuration, inlet 4, has a final monitor point temperature that is 13.71 K below the worst configuration and a volume averaged temperature that is 10.32 K below the worst configuration. A significant consequence of the preceding findings is that under both cold and hot conditions, better results are achieved with a lower inlet location.

A different set of data that is indicative of the effectiveness of the heating or cooling ability of a given configuration is given in the tables below. These tables show the difference between the final temperature and the comfort condition, as given by the equation below:

$$\Delta T = T_{final} - T_{comfort} = T_{final} - 295 \qquad (25)$$

Table 9 shows the final temperature reached at the monitor point in the transient test for each configuration under hot conditions while Table 10 gives the volume averaged temperature for the same time and conditions. Similarly, Table 11 and Table 12 provide the final monitor point temperature and volume averaged temperature at the end of the transient simulation under cold conditions. Because the comfort condition was never reached under cold conditions, there is only one table, Table 13, that shows the time required to reach the comfort condition.

Table 9: Final monitor point ΔT for hot conditions.

Inlet → / Outlet ↓	1	2	3	4	5
1	0.43	3.69	0.40	-1.84	2.92
2	11.70	2.25	-1.21	-2.02	-1.72
3	11.77	7.69	4.90	-1.67	-0.57
4	9.98	8.48	10.65	12.59	12.56
5	0.38	6.45	5.37	12.31	12.23

Table 10: Volume averaged ΔT for hot conditions.

Inlet → / Outlet ↓	1	2	3	4	5
1	0.39	3.92	2.26	1.85	3.52
2	11.56	3.25	2.15	1.24	2.05
3	11.64	8.41	9.00	5.61	5.61
4	11.20	8.78	10.82	11.80	11.95
5	0.33	6.69	8.34	10.31	11.35

Table 11: Final monitor point ΔT for cold conditions.

Inlet → / Outlet ↓	1	2	3	4	5
1	-7.10	-9.00	-9.00	-7.07	----
2	-9.00	-9.00	-7.20	-6.98	-3.84
3	-9.00	-9.00	-8.96	-7.50	-3.73
4	----	-6.71	-1.41	-6.83	-3.05
5	-6.86	-3.97	-1.65	-6.34	-2.46

Table 12: Volume averaged ΔT for cold conditions.

Inlet → / Outlet ↓	1	2	3	4	5
1	-5.42	-10.99	-7.96	-6.97	----
2	-10.97	-9.78	-6.10	-6.74	-3.94
3	-6.18	-6.08	-5.73	-7.12	-3.46
4	----	-3.93	-1.74	-6.87	-2.99
5	-4.13	-2.48	-1.14	-6.29	-2.56

Table 13: Time to reach comfort condition, 295 K, for hot conditions.

Inlet → / Outlet ↓	1	2	3	4	5
1	----	----	----	17.2	----
2	----	----	14.8	12.4	16.1
3	----	----	----	12.4	20.6
4	----	----	----	----	----
5	----	----	----	----	----

Under hot conditions, a more negative difference in the tables above was considered to show more effective cooling. This is because the more negative the difference was, the lower the final temperature was below the comfort condition. Since the cooling system could simply be turned off before reaching temperatures below the comfort condition, a more negative difference also meant that the system would not have to operate as much to maintain thermal comfort. On the other hand, under cold conditions, the less negative the final temperature given in the tables was, the better the heating performance was considered to be. Because all of the cold conditions have the same heating input, a more negative final difference shows a smaller effect of heating on the model and therefore a less effective heating configuration. The tables have been highlighted to exhibit the configurations that performed the best; the green cells indicate that the configuration resulted in a temperature that was better than the comfort condition while the yellow cells indicate that the configuration resulted in temperatures that were near the comfort condition.

The monitor point temperature data for the remaining test configurations can be seen in Appendix A.

5 Conclusions

While keeping either the inlet of the outlet location constant can help in determining trends in the results, it also helps to look at the complete data set. The transient monitor points were used to compare the amount of time required to attain the comfort condition. If the comfort condition was not attained, the data was still used to verify if the temperature had reached a steady state or if it was still in a transient mode. The most favorable result was considered to be one in which a steady state was reached at or near the comfort condition. Figure 17 below presents a matrix of monitor point temperature outputs for the duration of the transient tests.

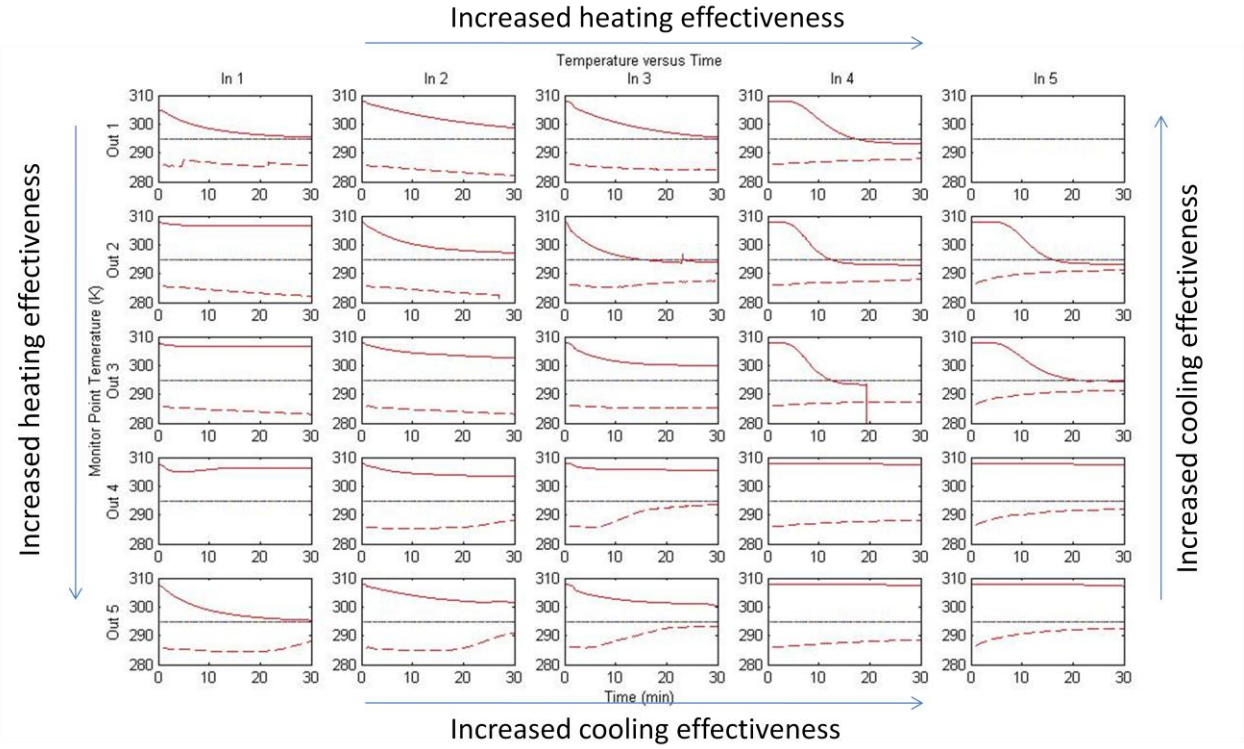

Figure 17: Transient temperature at monitor point for all configurations.

As is indicated in the above figure and Tables 8 through 12, a higher outlet exhibits better cooling while a lower outlet provides better heating. Furthermore, with a high outlet, the cooling effectiveness is improved with a higher inlet. At the same time, with a lower positioned outlet, a lower inlet seems to demonstrate better cooling. However, when only comparing the results of the two lowest outlet

positions, outlets four and five, another observation may be made; in nearly every case, outlet five exhibits better performance than outlet four. The cause of this trend can be determined from studying the flow patterns shown in Figure 18 and Figure 19. As the air from the inlets flows down the left wall because of the natural convective forces and is then diverted to the right by the floor, it proceeds to stream over the outlet located on the floor, outlet five. The flow then curls up the wall and is allowed to mix and fill the room. On the other hand, when the outlet is low on the right wall, at outlet four, the flow passes over the floor and is channeled directly into the outlet. This prevents the flow from mixing with the room air and thus reduces the effectiveness of the heating or cooling.

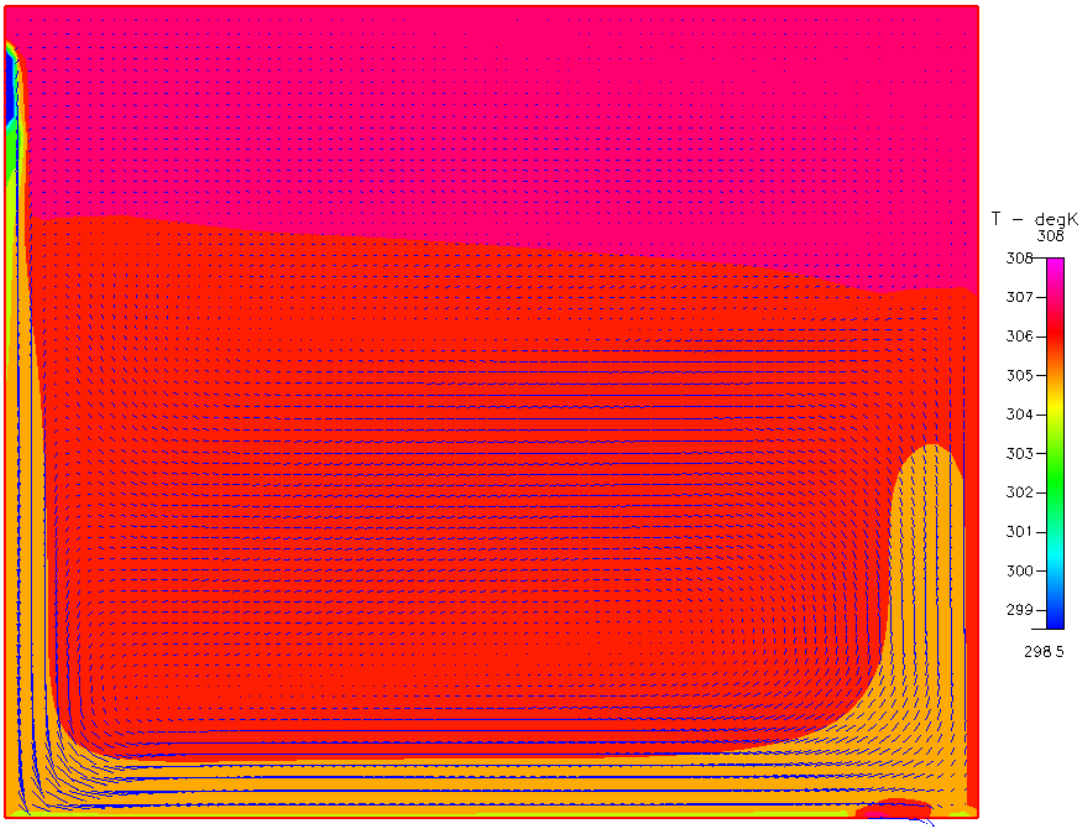

Figure 18: Configuration 2-5, cooling at 2.5 minutes into transient.

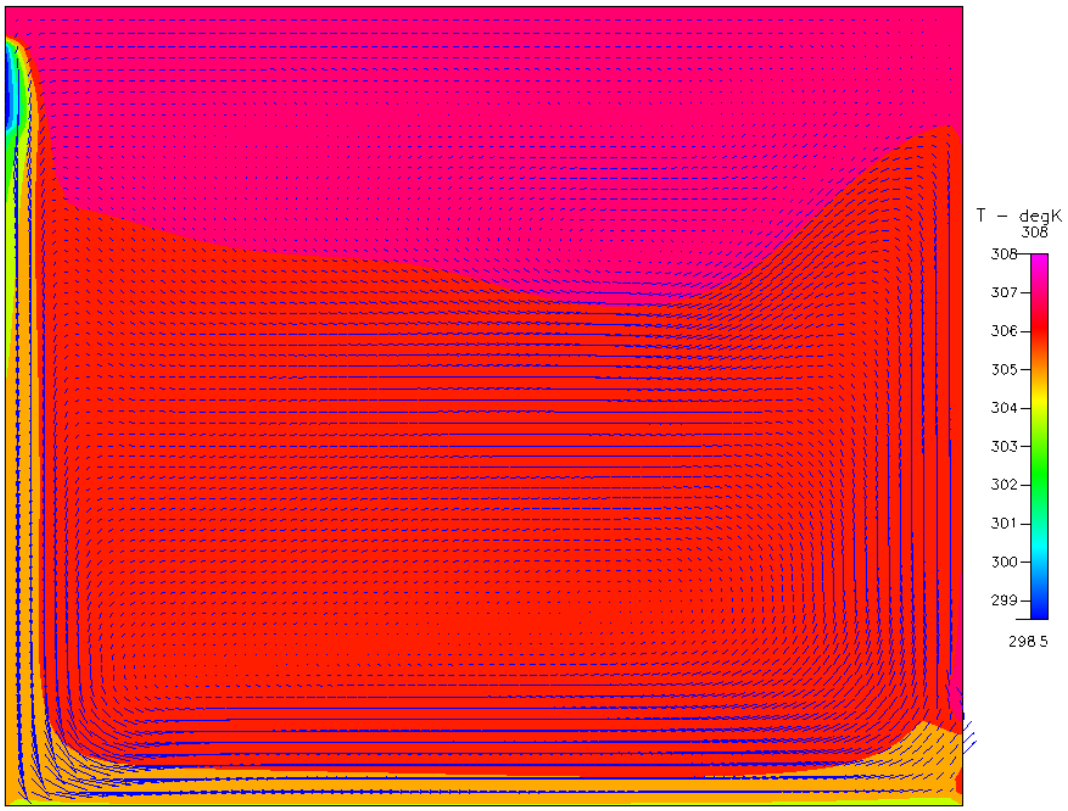

Figure 19: Configuration 2-4, cooling at 2.5 minutes into transient.

On the other hand, when only considering the two outlets near the top, outlets one and two, outlet two, which is located on the side wall yields better results. This is caused because the air that curls up the right wall after being diverted from the bottom corner flows parallel to the outlet; a smaller fraction of this flow escapes before it is allowed to mix with the room air.

It is clear that the mode of operation, heating or cooling, significantly affects the temperature distribution and flow patterns within the room. At the same time, there is no single configuration that reached the comfort condition under both modes of operation. Nevertheless, it was shown that a low inlet generally yields better performance for heating and cooling and the configurations that showed the best results were with inlet five and outlet two or three.

However, these results may not be best suited for every design scenario. Depending on energy usage patterns and geographical location or expected seasonal temperatures, one may desire to design

a system such that it is optimized for either heating or cooling. If the environmental temperatures are typically cold and heating is the main energy use, the use of a low, wall oriented inlet with a low, wall oriented outlet would be ideal. Conversely, if the environment is characteristically warmer and cooling will be more often used, an inlet that is centrally located on the height of a wall coupled with a high wall mounted outlet would be expected to yield the most desirable results.

With regard to the steady state investigation of the three-dimensional model, the data that was generated was not deemed viable because of the high residuals after evaluation. Accordingly, no reasonable conclusions can be drawn directly from these cases. However, it has been speculated that many of these model configurations do not actually have a steady state solution due to the effects of natural convection. Consequently, it would be necessary to run the simulations as transient in order to yield viable data.

6 Recommendations

While the original objective of this research was to use three-dimensional CFD analysis to determine a set of principles to guide the design of heating and cooling systems, many difficulties were encountered in devising, evaluating, and validating a three-dimensional model. As such, this leaves much room for future work in this area. Not only do problems such as computational limits and times complicate the matter of performing a three-dimensional investigation, but the sheer number of possible model configurations makes the development of a meaningful model more difficult as there are unlimited variations of actual physical room designs. Additionally, while a single model may be able to provide insights into the temperature and flow patterns within a room, changes as simple as an open doorway or any obstruction added within the room could dramatically affect the observed patterns within a physical building.

Areas of interest in future simulations would include changing of vent locations and changing of air injection methods. For example, a pulsed injection with a mean volumetric flow equal to the injection flow rate of a steady flow may offer more mixing and better results. Also, changing the number of inlets and outlets that are active in any given case may yield desirable results.

Appendix A

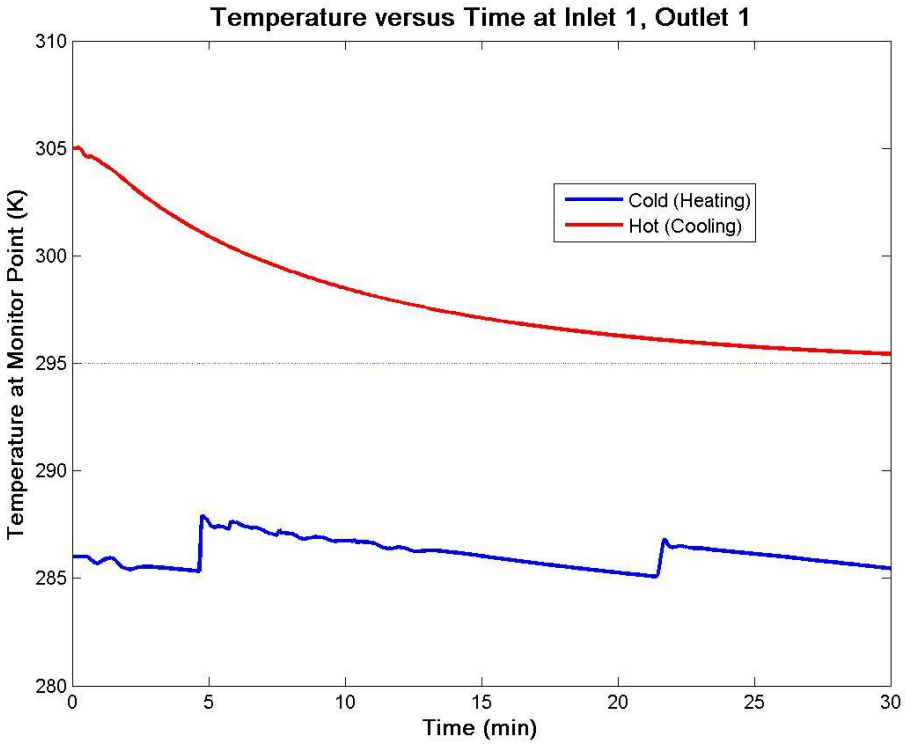
Temperature versus Time at Inlet 1, Outlet 1
Temperature at Monitor Point (K)
Time (min)
Cold (Heating)
Hot (Cooling)
310
305
300
295
290
285
280
0
5
10
15
20
25
30

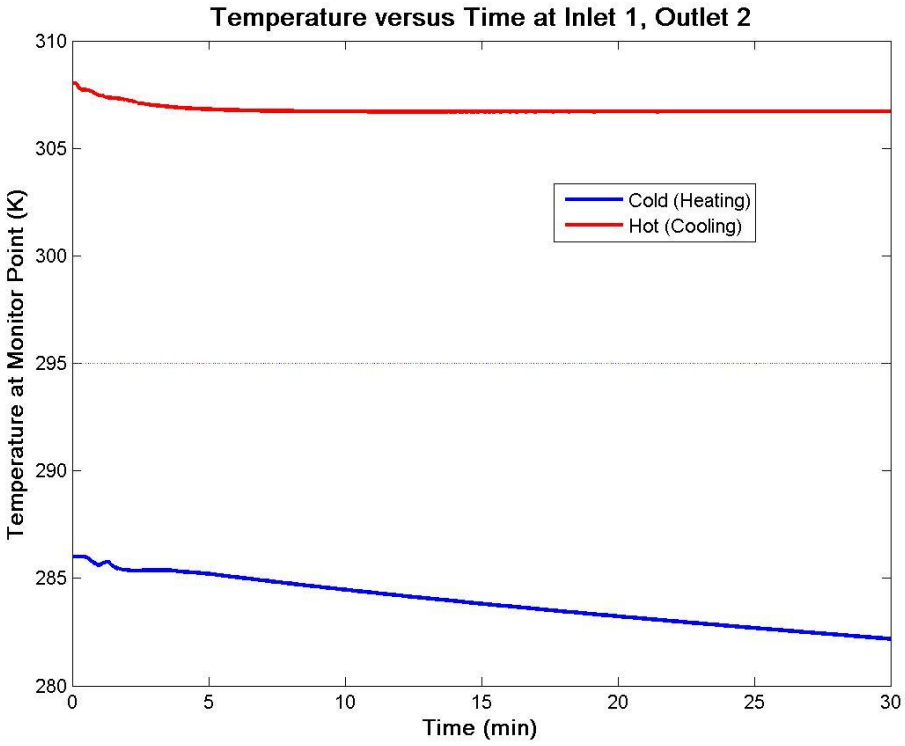
Temperature versus Time at Inlet 1, Outlet 2
Temperature at Monitor Point (K)
Time (min)
Cold (Heating)
Hot (Cooling)
310
305
300
295
290
285
280
0
5
10
15
20
25
30

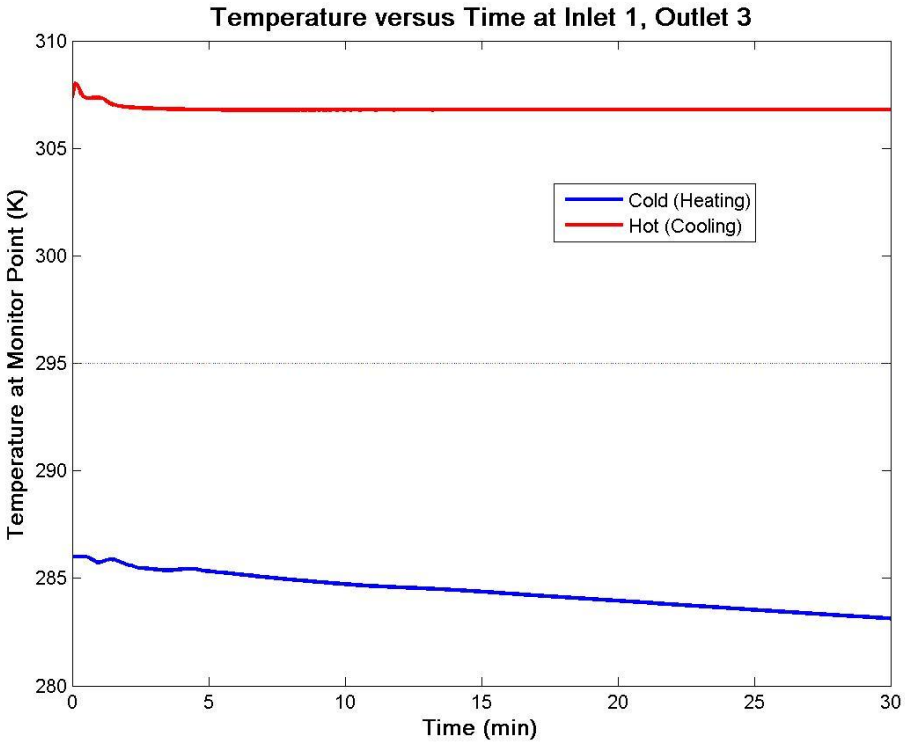
Temperature versus Time at Inlet 1, Outlet 3
Temperature at Monitor Point (K)
Time (min)
Cold (Heating)
Hot (Cooling)
310
305
300
295
290
285
280
0
5
10
15
20
25
30

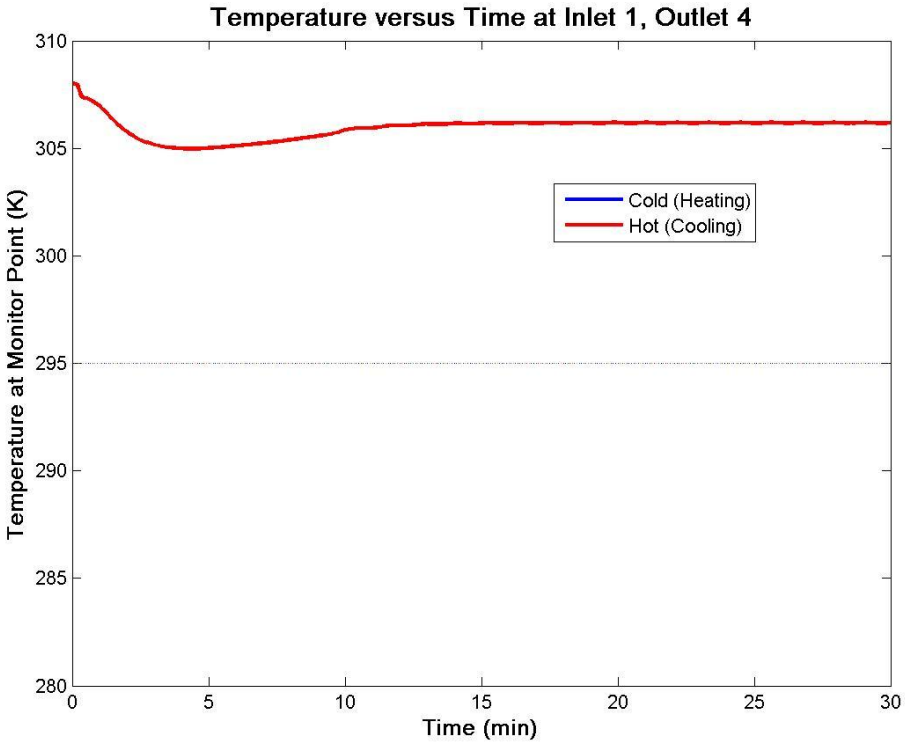
Temperature versus Time at Inlet 1, Outlet 4
Temperature at Monitor Point (K)
Time (min)
Cold (Heating)
Hot (Cooling)
310
305
300
295
290
285
280
0
5
10
15
20
25
30

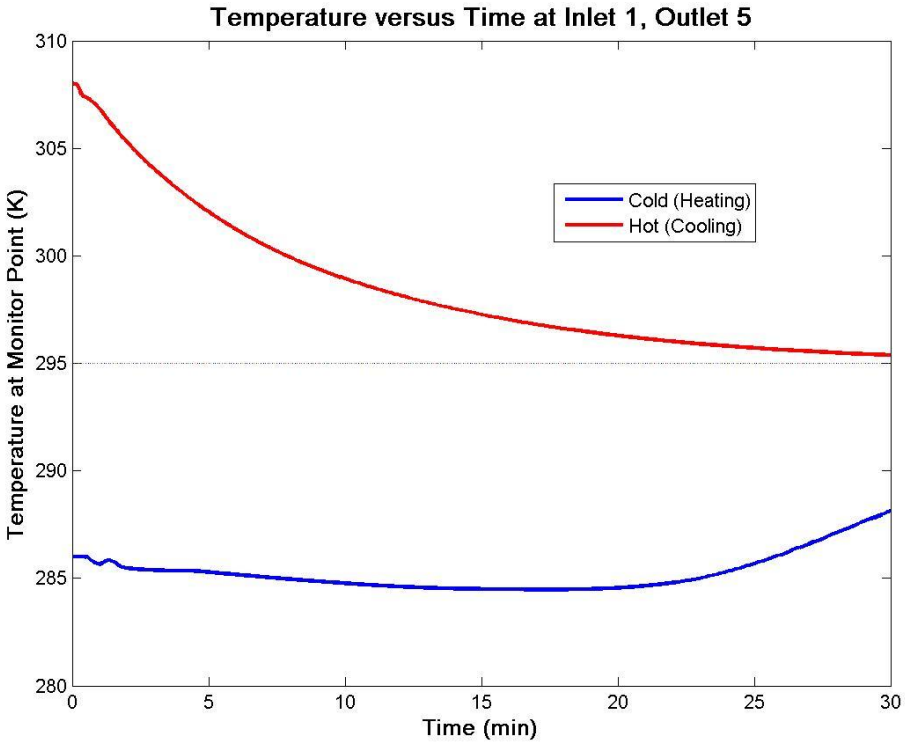
Temperature versus Time at Inlet 1, Outlet 5
Temperature at Monitor Point (K)
Time (min)
Cold (Heating)
Hot (Cooling)
310
305
300
295
290
285
280
0
5
10
15
20
25
30

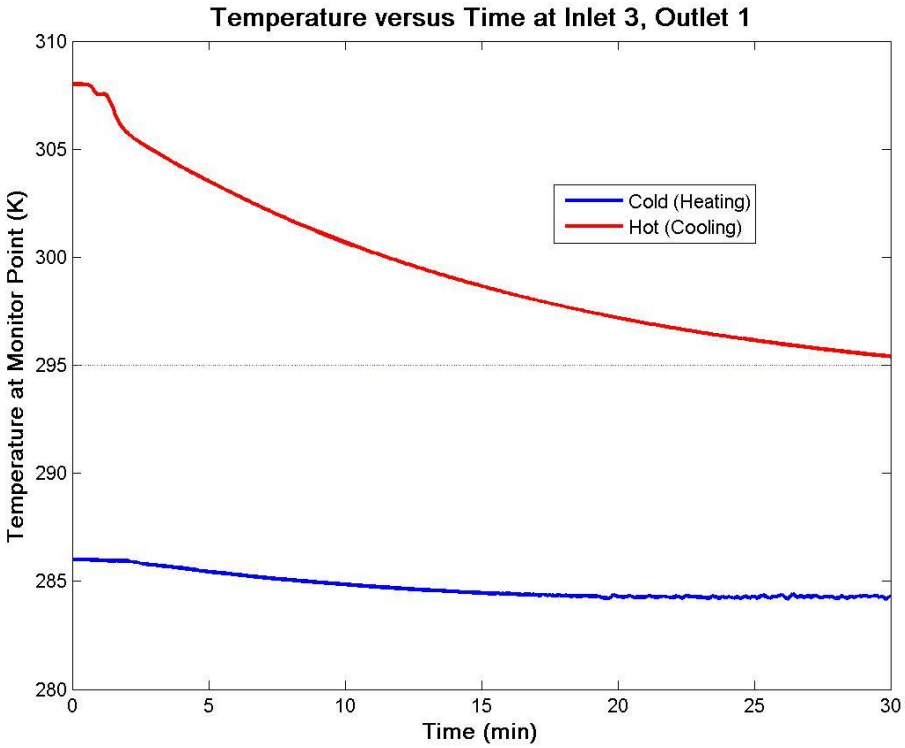
Temperature versus Time at Inlet 3, Outlet 1
Temperature at Monitor Point (K)
Time (min)
Cold (Heating)
Hot (Cooling)
310
305
300
295
290
285
280
0
5
10
15
20
25
30

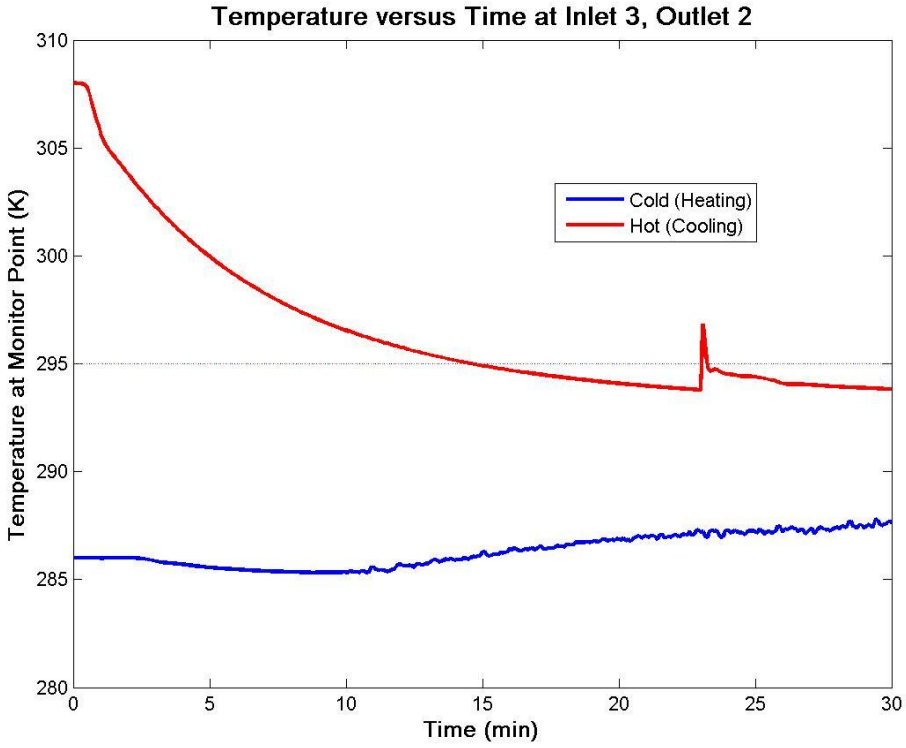
Temperature versus Time at Inlet 3, Outlet 2
Temperature at Monitor Point (K)
Time (min)
Cold (Heating)
Hot (Cooling)
310
305
300
295
290
285
280
0
5
10
15
20
25
30

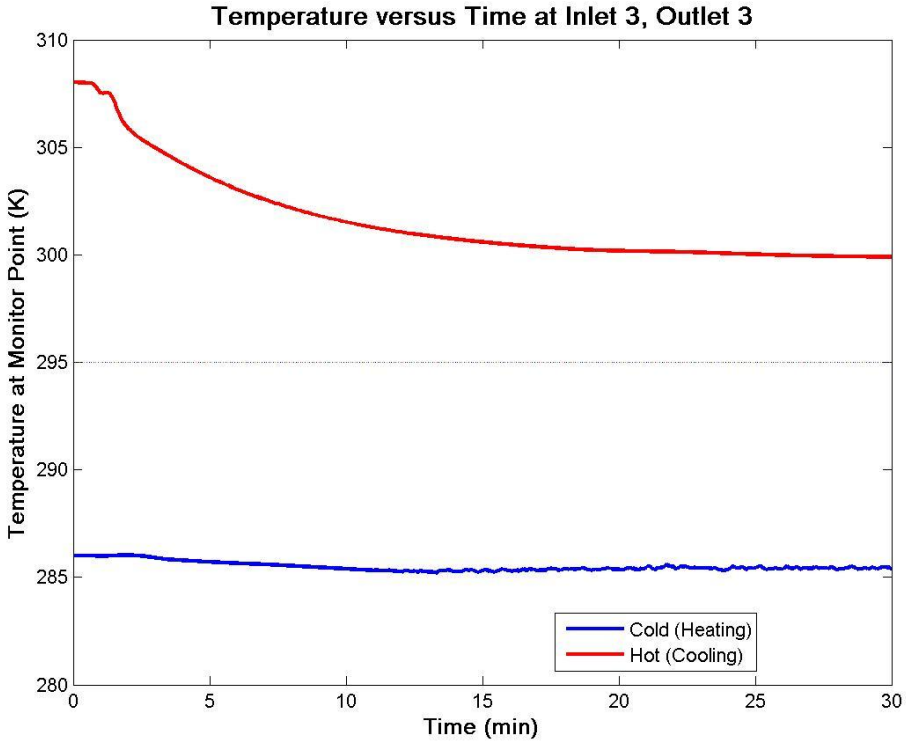
Temperature versus Time at Inlet 3, Outlet 3
Temperature at Monitor Point (K)
Time (min)
Cold (Heating)
Hot (Cooling)
310
305
300
295
290
285
280
0
5
10
15
20
25
30

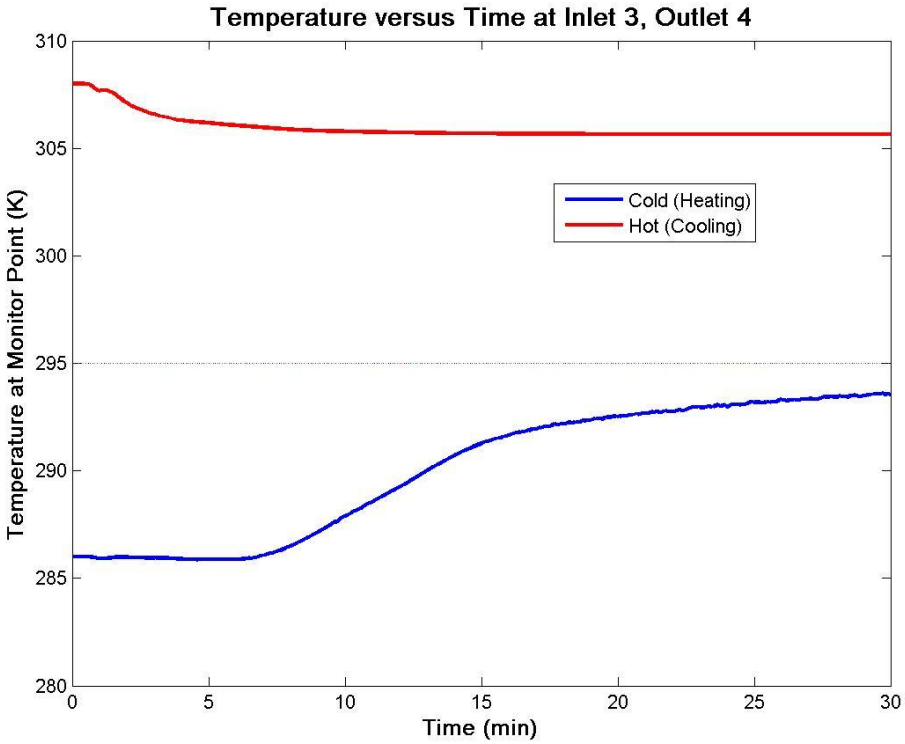
Temperature versus Time at Inlet 3, Outlet 4
Temperature at Monitor Point (K)
Time (min)
Cold (Heating)
Hot (Cooling)
310
305
300
295
290
285
280
0
5
10
15
20
25
30

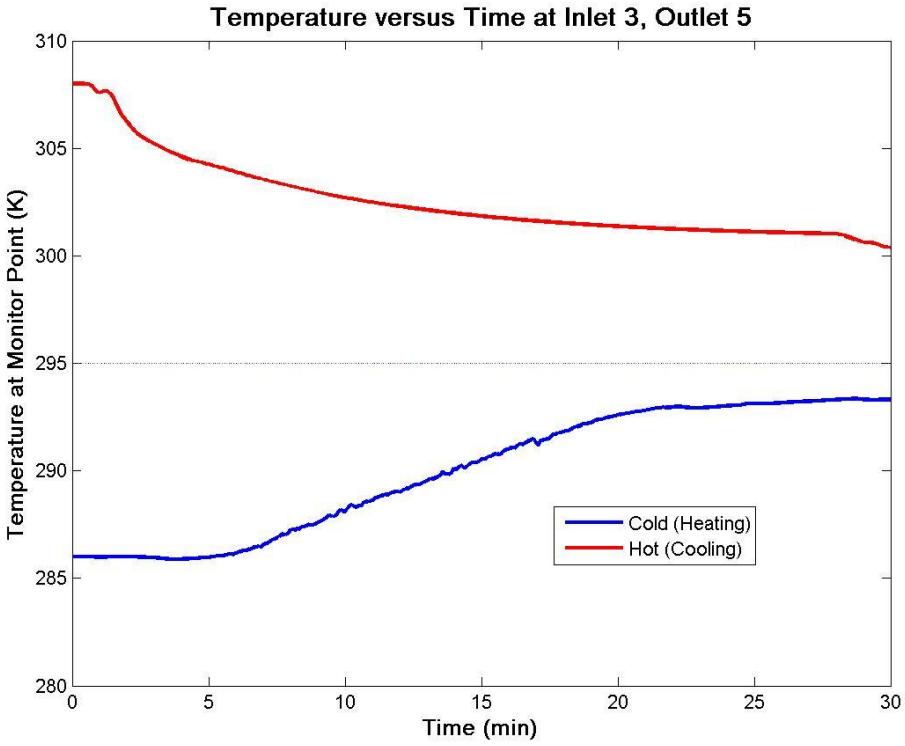
Temperature versus Time at Inlet 3, Outlet 5
Temperature at Monitor Point (K)
Time (min)
Cold (Heating)
Hot (Cooling)
310
305
300
295
290
285
280
0
5
10
15
20
25
30

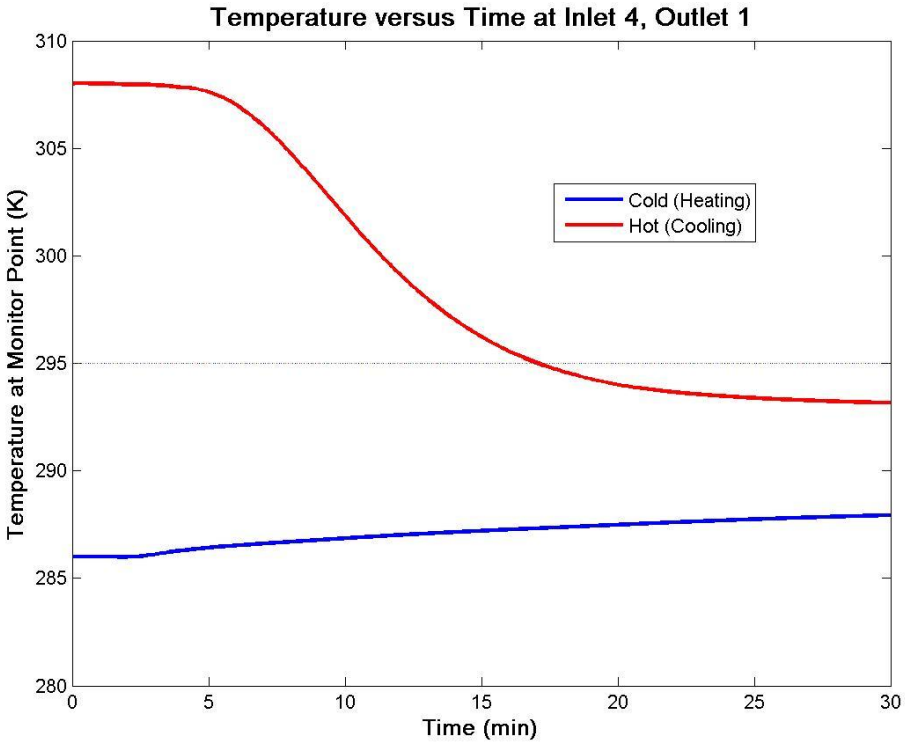
Temperature versus Time at Inlet 4, Outlet 1
Temperature at Monitor Point (K)
Time (min)
Cold (Heating)
Hot (Cooling)
310
305
300
295
290
285
280
0
5
10
15
20
25
30

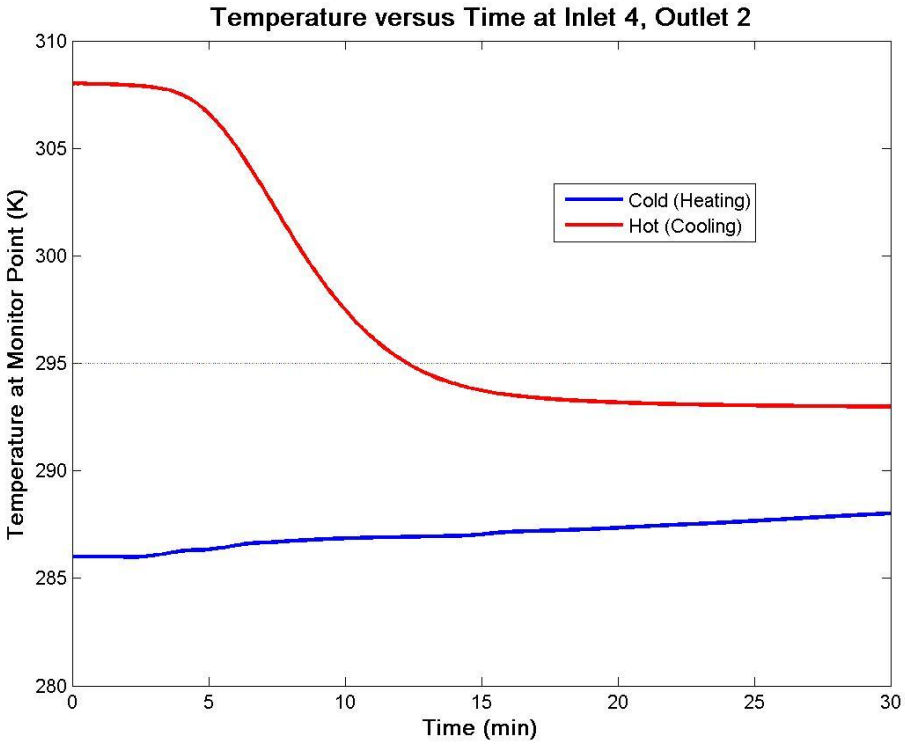
Temperature versus Time at Inlet 4, Outlet 2
Temperature at Monitor Point (K)
Time (min)
Cold (Heating)
Hot (Cooling)
310
305
300
295
290
285
280
0
5
10
15
20
25
30

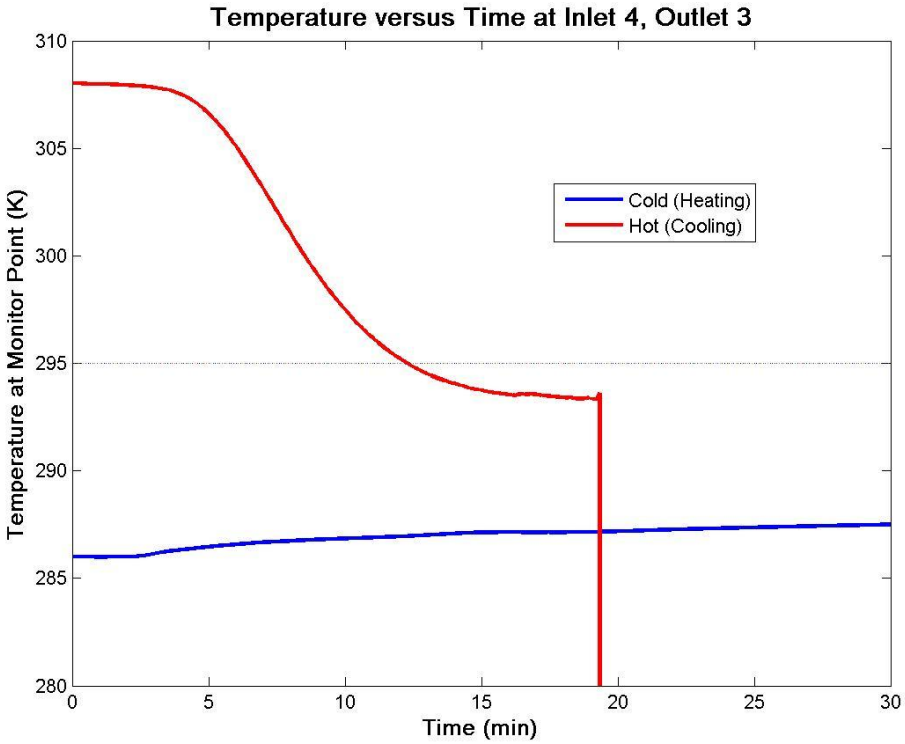
Temperature versus Time at Inlet 4, Outlet 3
Temperature at Monitor Point (K)
Time (min)
Cold (Heating)
Hot (Cooling)
310
305
300
295
290
285
280
0
5
10
15
20
25
30

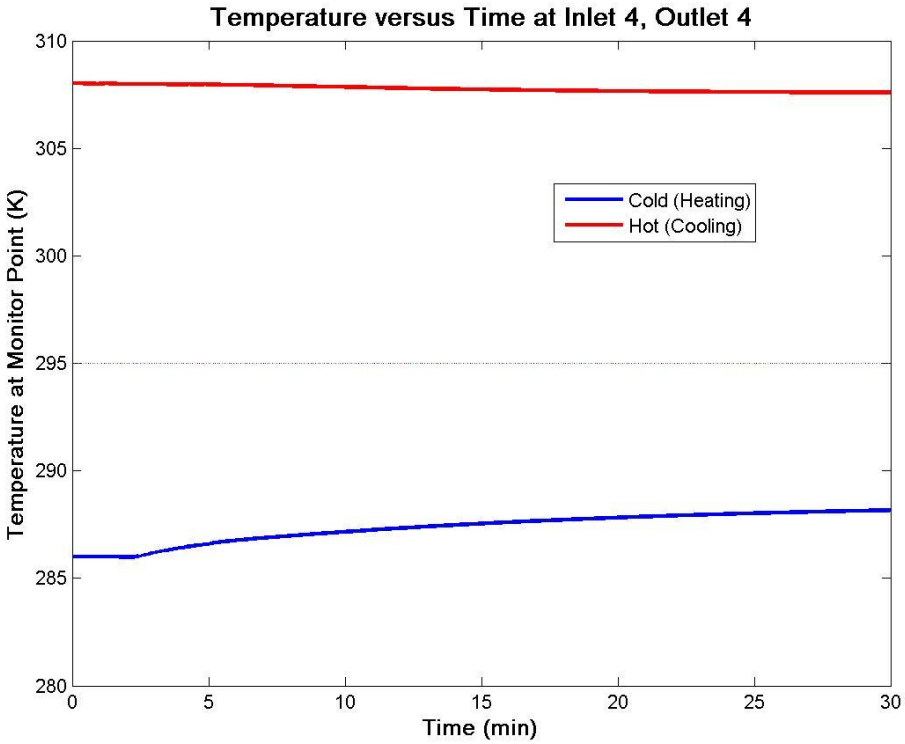
Temperature versus Time at Inlet 4, Outlet 4
Temperature at Monitor Point (K)
Time (min)
Cold (Heating)
Hot (Cooling)
310
305
300
295
290
285
280
0
5
10
15
20
25
30

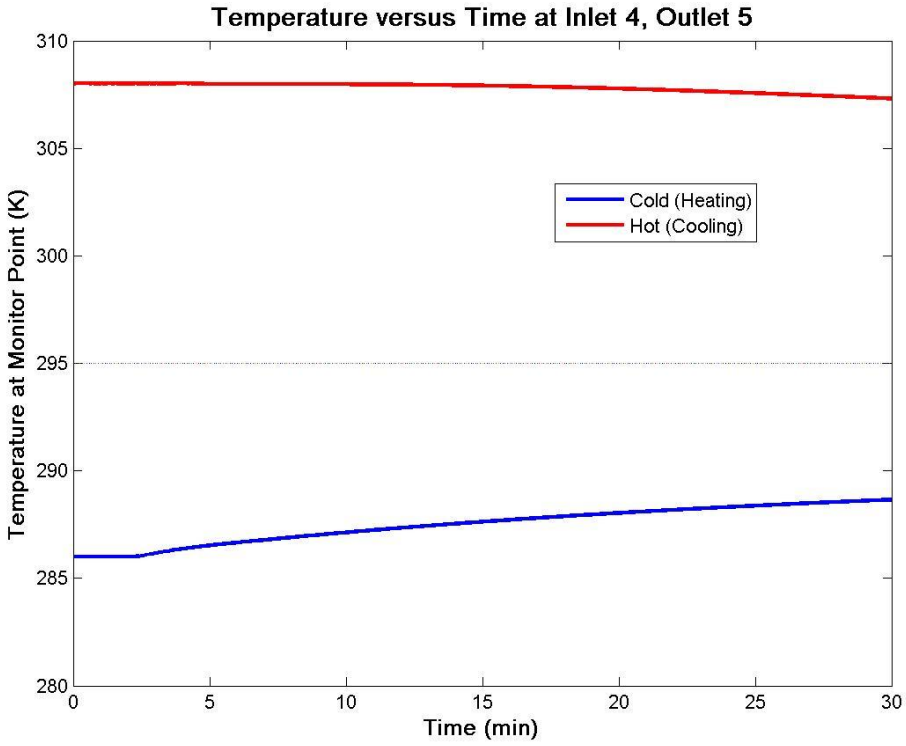
Temperature versus Time at Inlet 4, Outlet 5
Temperature at Monitor Point (K)
Time (min)
Cold (Heating)
Hot (Cooling)
310
305
300
295
290
285
280
0
5
10
15
20
25
30

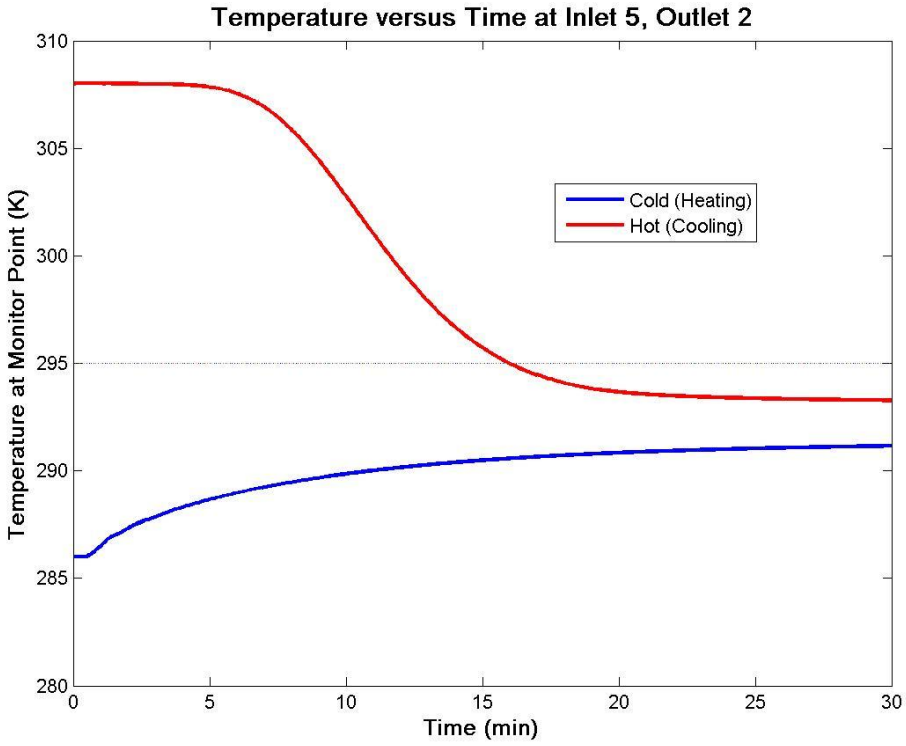
Temperature versus Time at Inlet 5, Outlet 2
Temperature at Monitor Point (K)
Time (min)
Cold (Heating)
Hot (Cooling)
310
305
300
295
290
285
280
0
5
10
15
20
25
30

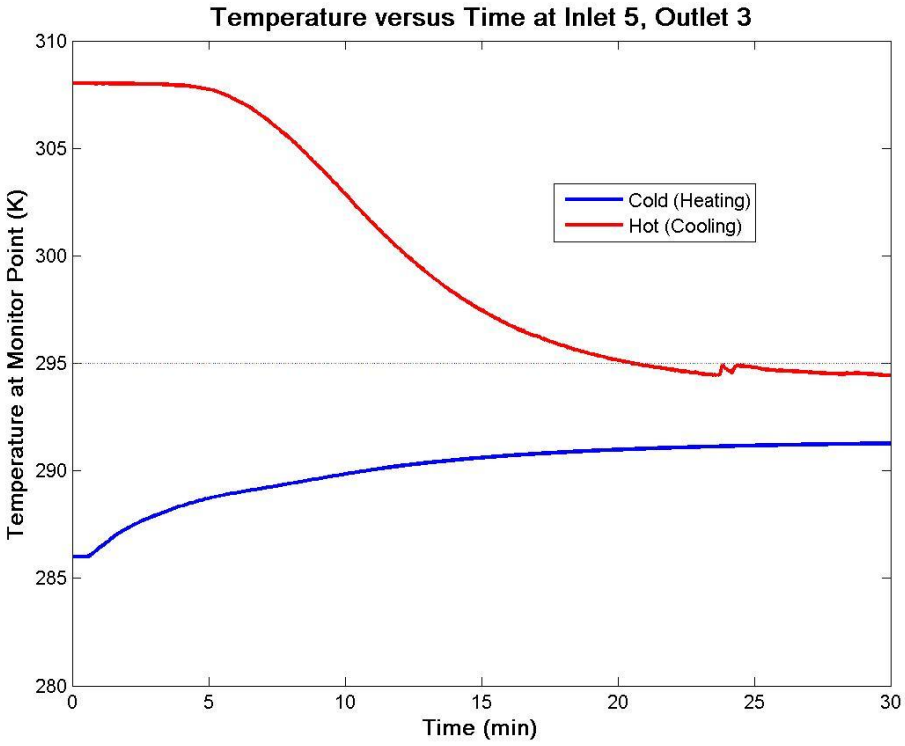
Temperature versus Time at Inlet 5, Outlet 3
Temperature at Monitor Point (K)
Time (min)
Cold (Heating)
Hot (Cooling)
310
305
300
295
290
285
280
0
5
10
15
20
25
30

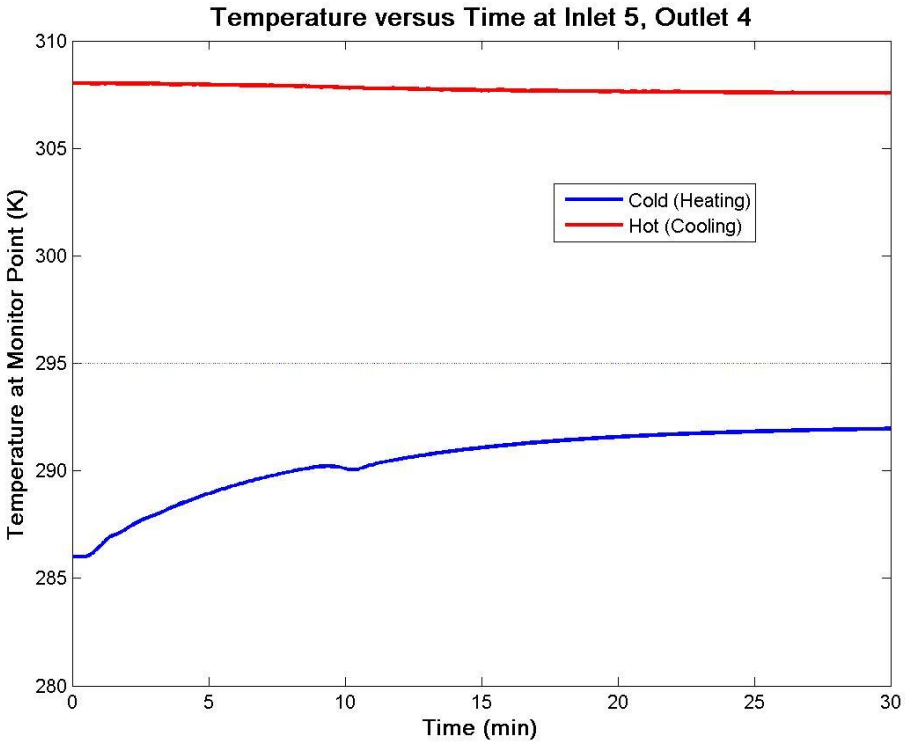
Temperature versus Time at Inlet 5, Outlet 4
Temperature at Monitor Point (K)
Time (min)
Cold (Heating)
Hot (Cooling)
310
305
300
295
290
285
280
0
5
10
15
20
25
30

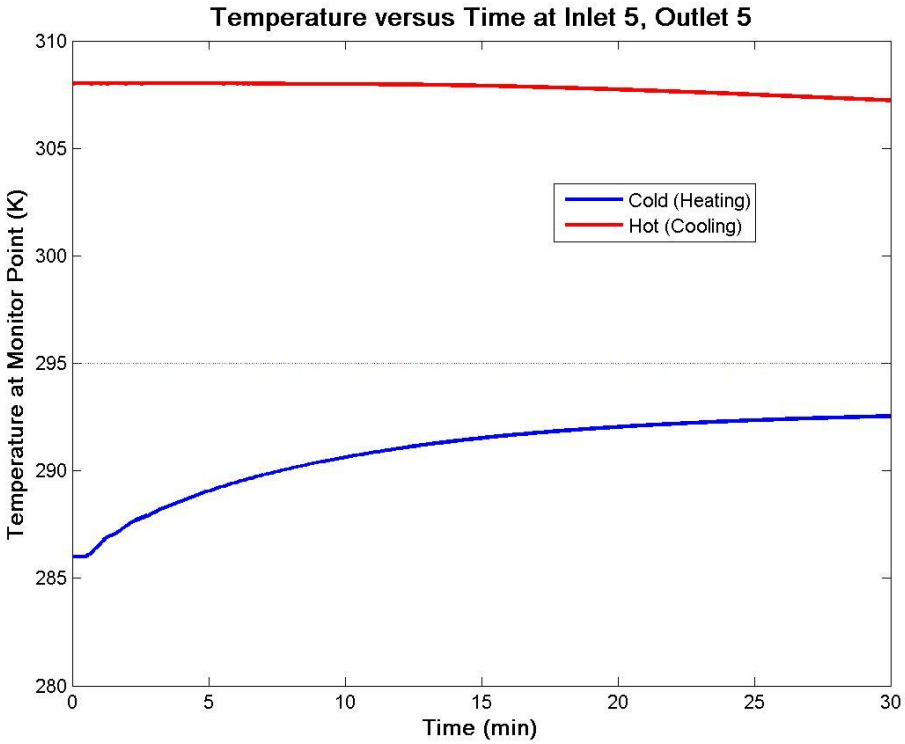
Temperature versus Time at Inlet 5, Outlet 5
Temperature at Monitor Point (K)
Time (min)
Cold (Heating)
Hot (Cooling)
310
305
300
295
290
285
280
0
5
10
15
20
25
30

Bibliography

CFD-ACE+. s.l. : ESI Inc. www.esi-group-na.com.

Chung, K. C. 1999. Three-Dimensional analysis of airflow and contaminant particale transport in a partitioned enclosure. *Building and Environment.* 34, 1999.

Incropera, et al. 2007. Introduction to Heat Transfer. Davers, MA : John Wiley & Sons, 2007.

Residential Energy Consumption Survey (RECS). [Online] U.S. Energy Information Administration. http://www.eia.doe.gov/consumption/residential/reports/electronics.cfm.

Zhongwei Sun, Shengwei Wang. 2010. A CFD-based method for control of indoor environment and space ventilation. *Building and Environment.* 45, 2010.